

Scaling relations for galaxy clusters: properties and evolution

Giodini, S. · Lovisari, L. · Pointecouteau,
E. · Etti, S. · Reiprich, T. H. · Hoekstra,
H.

Received: date / Accepted: date

Abstract Well-calibrated scaling relations between the observable properties and the total masses of clusters of galaxies are important for understanding the physical processes that give rise to these relations. They are also a critical ingredient for studies that aim to constrain cosmological parameters using galaxy clusters. For this reason much effort has been spent during the last decade to better understand and interpret relations of the properties of the intra-cluster medium. Improved X-ray data have expanded the mass range down to galaxy groups, whereas SZ surveys have opened a new observational window on the intracluster medium. In addition, continued progress in the performance of cosmological simulations has allowed a better understanding of the physical processes and selection effects affecting the observed scaling relations. Here we review the recent literature on various scaling relations, focussing on the latest observational measurements and the progress in our understanding of the deviations from self similarity.

S. Giodini
Leiden Observatory, Leiden University, PO Box 9513, 2300 RA Leiden, the Netherlands
TNO, Acoustic and Sonar, Oude Waalsdorperweg 63, 2597AK The Hague, the Netherlands
E-mail: stefania.giodini@tno.nl

L. Lovisari
Argelander-Institut für Astronomie, Bonn University, Auf dem Hügel 71, 53121 Bonn, Germany

E. Pointecouteau
Université de Toulouse, CNRS, CESR, 9 av. du colonel Roche, BP 44346, 31028, Toulouse
Cedex 04, France

S. Etti
INAF-Osservatorio Astronomico, via Ranzani 1, 40127 Bologna, Italy
INFN, Sezione di Bologna, viale Berti Pichat 6/2, 40127 Bologna, Italy

T. H. Reiprich
Argelander-Institut für Astronomie, Bonn University, Auf dem Hügel 71, 53121 Bonn, Germany

H. Hoekstra
Leiden Observatory, Leiden University, PO Box 9513, 2300 RA Leiden, the Netherlands

Keywords Galaxy clusters · large-scale structure of the Universe · intracluster matter

1 Introduction

In our current paradigm of structure formation, tiny density fluctuations rise and grow in the early Universe under the influence of gravity, to create the massive, dark matter dominated structures we observe today. Clusters of galaxies correspond to the densest regions of the resulting large-scale structure. The spatial distribution and number density of clusters carries the imprint of the process of structure formation and, as a consequence, these properties are sensitive to the underlying cosmological parameters. This strong dependence of the evolution of the halo mass function at the cluster scale on the cosmology is shown in Fig. 1, which gives a convincing visual example of why clusters of galaxies attractive probes of cosmology. and have been suggested as a potential probe of the dark energy equation of state (e.g. Schuecker et al. 2003; Albrecht et al. 2006; Henry et al. 2009; Vikhlinin et al. 2009a,2009b; Mantz et al. 2010b; Allen et al. 2011). Results from these studies are consistent with other observations that indicate a Universe dominated by dark energy ($\sim 73\%$), with sub-dominant dark matter ($\sim 23\%$), and a relatively small amount of baryonic material ($\sim 4.5\%$) (Komatsu et al. 2011).

In order to use cluster number counting to constrain cosmological parameters, accurate knowledge of their total mass is a crucial ingredient. Masses can be measured directly by means of weak and strong lensing (see Hoekstra et al. 2013, in this volume) or, under the assumption of virial equilibrium, through measurements of the velocity dispersion of the cluster galaxies. Obtaining individual mass measurements for a large number of system is observationally very expensive. Instead it is of interest to rely on robust and well understood scaling relations that are able to relate the total mass to quantities that are more easily observed.

These relations are the result of the physics of cluster formation and evolution. If gravity is the dominant process, the resulting self-similar models predict simple scaling relations between basic cluster properties and the total mass (Kaiser 1986). Three correlations are particularly important, namely the X-ray luminosity–temperature, mass–temperature and luminosity–mass relations. In general these are described as power laws in the average, around which points scatter according to a lognormal distribution. These relations describe positive correlations, with the larger systems having on average more of everything. Hence scaling relations are not merely a tool for cosmology but are also precious diagnostics to study the thermodynamical history of the intra-cluster medium (ICM).

With the advent of large, deep surveys of galaxy groups below temperatures of 4 keV, a number of observational studies have reported deviations from the self-similar scaling relations for low mass systems (e.g. Gastaldello et al. 2007; Sun et al. 2009; Eckmiller et al. 2011). Such deviations indicate that non-gravitational processes may be a significant contributor to the global energy budget in clusters. These findings have triggered an interest from the scientific community working on cosmological simulations to take such processes into account. Nowadays many cosmological simulations include prescriptions for non-gravitational processes such as pre-heating during collapse (due to star formation or shocks), radiative cooling and feedback by super-massive black holes. There is general agreement that these processes need to be included in order to reproduce the observed scaling relations. The relative contributions of the various

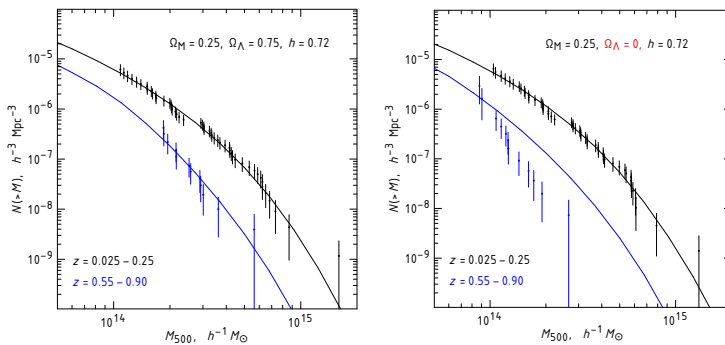


Fig. 1 Illustration of sensitivity of the cluster mass function to the cosmological model (taken from Vikhlinin et al. 2009a). In the left panel the measured mass function and predicted models are shown. In the right panel, both the data and the models are computed for a cosmology with $\Omega_{\Lambda} = 0$. Both the model and the data at high redshifts are changed relative to the $\Omega_{\Lambda} = 0.75$ case. The measured mass function is changed because it is derived for a different distance-redshift relation. The model is changed because the predicted growth of structure and overdensity thresholds corresponding to $\Delta_{crit} = 500$ are different. When the overall model normalization is adjusted to the low- z mass function, the predicted number density of $z > 0.55$ clusters is in strong disagreement with the data, and therefore this combination of Ω_M and Ω_{Λ} can be rejected.

non-gravitational processes, however, are still a matter of debate and will remain a major subject of research for the next decade.

The need for a good mass tracer does not only require an understanding of the physics of individual galaxy clusters, but also of the cluster population as a whole. To understand the shape, evolution and intrinsic scatter in the scaling relations, representative populations need to be studied. Selecting galaxy clusters using their X-ray emission is an efficient way of identifying bound, evolved and virialized systems. In the last decade a large effort has been made to understand possible biases in this selection. Indeed flux limited surveys suffer from selection biases (in particular Malmquist bias), and additional complications have to be taken into account when considering the scatter or biases in the observables and the total mass determination.

A key advantage of the multi-component nature of galaxy clusters is the fact that they can be observed at different wavelengths (see Fig. 2). Therefore additional scaling relations that relate the cluster total mass to properties inferred from optical, infrared, submillimeter and radio observations, have been derived. These relations allow a deeper insight into the biases and selection effects which affect the X-ray based results. In particular samples of clusters observed in large Sunyaev-Zel'dovich (SZ) surveys are highly complementary to the X-ray ones because of the different scaling of SZ and X-ray fluxes with electron density and temperature. Furthermore, they are less biased towards clusters with cool cores. On the other hand, because of their current sensitivity limits, SZ samples are restricted to high mass systems ($M_{tot} > 10^{14} M_{\odot}$). It is therefore important to complement SZ and X-ray samples with those obtained from optical surveys. The latter are able to detect the lowest mass structures, even if they are not virialized, and thus give a more complete census of the large scale structure.

In this review we present an overview of the studies of scaling relations of a number of observables with the total mass (or its proxies), focusing mainly on results from the last decade. We start with X-ray relations in §2 and discuss their evolution in §3. The

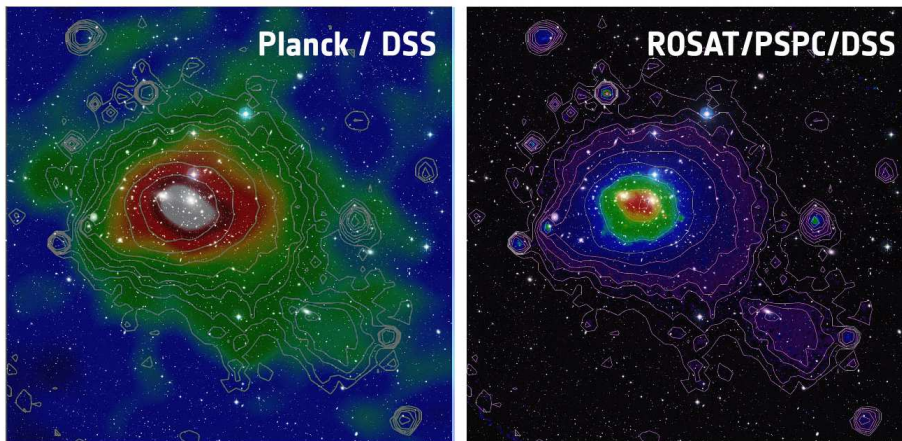


Fig. 2 The Coma cluster as seen by Planck (left) through the SZ effect and ROSAT (right) in X-rays. The images are overlaid on visible light images of the cluster obtained by DSS. *Image credits: ESA / LFI and HFI Consortia (Planck image); MPI (ROSAT image); NASA/ESA/DSS2 (visible image). Acknowledgement: Davide De Martin (ESA/Hubble)*

SZ results are reviewed in §4 and optical scaling relations in §5. The interpretation of observational results using simulations are discussed in §6. General considerations are discussed in §7 with conclusions and an outlook presented in §8.

2 X-ray relations

Before discussing observational constraints on X-ray scaling relations, it is useful to consider first what to expect in the case of simple models in which only gravity is important. As shown in Kaiser (1986) this leads to a so-called self-similar model, with power law scaling relations. In general an object is said to be self-similar when each portion of itself can be considered a reduced-scale image of the whole (Mandelbrot 1967). Mathematically speaking, a self-similar function is invariant under dilatation, such that

$$f(x) = f(\alpha x). \quad (1)$$

Power laws (i.e. $f(x) = x^n$) are typical functions for which self-similarity applies. Exact self-similarity is a typical property of fractals, such as the Koch curve or the Sierpiński gasket, where the rescaled system is identical to the original one for each rescaling length. Nature, instead, exhibits the property of *statistical* self-similarity, meaning that only statistical quantities are the same for the rescaled and the original system, and only for a range of scales; physical systems are considered self-similar if dimensionless statistics are invariant under rescaling.

We follow the arguments from Kaiser (1986), considering the case where the Universe has closure density (i.e., $\Omega = 1$). Under this assumption the initial spectrum of density fluctuations, $P(k)$, is a power law over some range of wave-number, such that

$$P(k) \propto k^n. \quad (2)$$

The mass variance of the fluctuations σ^2 scales as

$$\sigma^2(k) \sim k^3 P(k) \propto r^{-(n+3)} \propto M^{-(n+3)/3}, \quad (3)$$

where the last two proportionalities follow because $k \propto \frac{1}{r}$ and $M \propto r^3$. Therefore, under these conditions, the amplitude σ of the fluctuations is a power law function of the size or mass. Hence the fluctuations are self-similar. They grow in time leading to non-linear evolution when $\sigma = 1$. The growth of density fluctuations is described by

$$\sigma(M, t) \propto a(t) M^{-(n+3)/6}, \quad (4)$$

where $a(t)$ is the scale factor. When $\sigma = 1$ we obtain the scaling of the mass-scale of non-linearity, M_{NL} , given by

$$M_{\text{NL}} \propto a^{\frac{6}{(n+3)}}. \quad (5)$$

The transition from the linear to the non-linear regime is the only scale introduced in the problem and as a result all statistical quantities of the evolved fluctuation field (i.e. the number density of halos of a given mass at time t), depend on the ratio M/M_{NL} only. In other words, M_{NL} is a characteristic variable that captures the dependence on the normalization and shape of the matter power spectrum¹. With the power spectrum specified, the only dependence a function of M/M_{NL} can have is on $a(t)$, which itself is a power law of time (i.e. $a \propto t^{2/3}$). This implies that the function is self-similar with respect to time. For example, the halo properties and halo abundance of two structures which have the same M/M_{NL} at two different times are the same.

In general, the statistical properties of haloes are expressed as a function of the density contrast $\Delta(r, t)$ at a given time and (comoving) scale, with $\Delta \propto a(t)^{-2/3}$. The statistic $S(\Delta)$ obeys self-similarity, so that

$$S(\Delta(r, t_1)) = S(\Delta(r, t_2)) = S(\Delta(a(t_2)r)). \quad (6)$$

In this sense, a universe starting from a power-law power spectrum is defined as self-similar. As discussed by Kaiser (1986), this power-law shape cannot be expected at all scales, but it is a good approximation on the scales of galaxy clusters and groups.

2.1 Self-similar scaling relations for galaxy clusters

The argument for self-similarity holds for collisionless particles, such as dark matter, because gravity is the only force acting on the particles. Gas in galaxy clusters can be considered "weakly collisional" since the ion Larmor radius is much smaller than the mean free Coulomb path (10^8 cm versus 10-30 kpc for a typical density of $n \sim 10^{-3} \text{cm}^{-3}$, e.g. Lyutikov 2007). Numerical simulations (e.g. Navarro et al. 1995) have shown that self-similarity holds also for the gas component if the effects of gravity and shock heating are included, neglecting any of the dissipative, non-gravitational effects. This means that when observing collapsed structures such as galaxy clusters, provided dissipation can be neglected, their dimensionless properties (e.g. their gas fraction, temperature distribution, etc.) can be expected to be self-similar in time and $M_{\text{gas}, \Delta} \propto M_{\text{DM}, \Delta}$ (Kaiser 1986). As a consequence, in a hierarchical scenario, where

¹ M_{NL} is the variable of choice when the power spectrum is a power law of k . When this is not the case, other choices are more adequate.

small structures form first and provide the building blocks for larger ones, these small structures are expected to be scaled down versions of the big ones.

In such a self-similar universe several simple relations between the X-ray properties of the gas can be predicted. Since structures are self-similar in time, two haloes that have formed at the same time must have the same mean density. Hence

$$\frac{M_{\Delta_z}}{R_{\Delta_z}^3} = \text{constant}, \quad (7)$$

where R_{Δ_z} is the radius where the density contrast² is Δ_z . M_{Δ_z} is the mass within a sphere of radius R_{Δ_z} defined as:

$$M_{\Delta_z} = \frac{4\pi}{3} \Delta_z \rho_{\text{crit},0} E_z^2 R_{\Delta_z}^3, \quad (8)$$

where $E_z = H_z/H_0 = [(\Omega_m(1+z)^3 + (1 - \Omega_m - \Omega_\Lambda)(1+z)^2 + \Omega_\Lambda)]^{1/2}$ describes the evolution of the Hubble parameter with redshift z . A cluster of galaxies is considered to be in hydrostatic equilibrium when the pressure gradient balances the gravitational force. If hydrostatic equilibrium holds, the temperature of the gas provides a good estimate of the depth of the potential well and thus of the virial mass of the cluster:

$$T_{\text{gas}} \propto \frac{GM}{R} \propto R_{\text{vir}}^2, \quad (9)$$

where R_{vir} is the virial radius. If we substitute Eqn. 7 into Eqn. 9 it follows that

$$M_{\Delta_z} \propto T_{\text{gas}}^{\frac{3}{2}}, \quad (10)$$

which is the expected scaling relation between mass and ICM temperature.

To relate the X-ray luminosity, which is easier to observe, to the temperature we need to assume an emission mechanism. For sufficiently massive systems the ICM is shock heated to temperatures of 10^7 - 10^8 K and emits mainly by thermal bremsstrahlung. In this emission regime (for a plasma with solar metallicity) the total emissivity ϵ (luminosity per unit volume) and the temperature are related as follows

$$\epsilon \simeq 3.0 \times 10^{-27} T_{\text{gas}}^{1/2} \rho_{\text{gas}}^2 \text{ erg cm}^{-3} \text{ s}^{-1}, \quad (11)$$

where we are implicitly assuming thermal equilibrium, such that the temperature of the electrons is the same as that of the ions. By means of Eqns. 10 and 11 it is then possible to relate the X-ray luminosity to the total mass:

$$L_X \approx \epsilon R_{\Delta_z}^3 \approx T_{\text{gas}}^{1/2} \rho_{\text{gas}}^2 R_{\Delta_z}^3 \approx T_{\text{gas}}^{1/2} f_{\text{gas}}^2 M_{\text{tot}} \approx f_{\text{gas}}^2 T_{\text{gas}}^2, \quad (12)$$

where f_{gas} is the gas fraction defined as $M_{\text{gas}}/M_{\text{tot}}$ and where we used the second proportionality in Eqn. 9 to obtain the last scaling. Since the gas fraction is predicted to be a constant in the self-similar scenario, this implies that (e.g. Ponman et al. 1999):

$$L_X \propto T_{\text{gas}}^2. \quad (13)$$

² The density contrast Δ is usually expressed with respect to the critical density at the cluster redshift. As detailed in Böhringer et al. (2012), the evolution of the background and critical density across the cosmic epoch introduces a redshift dependence in the definition of Δ . Indeed to relate clusters at different epoch and sizes the density contrast should be scaled as $\Delta_z = \Delta(z=0) \frac{\Delta_{\text{vir}}(z)}{\Delta_{\text{vir}}(z=0)}$.

Equations 10 and 13 are the basic scaling relations between X-ray properties in galaxy clusters predicted by the self-similar model. These hold for halo masses where dissipative processes can be ignored. Consequently, a departure from this prediction can be used to quantify the importance of non-gravitational processes.

We stress that the so-called *self-similar scenario* results from a property of the dark matter power spectrum of initial fluctuation and that it predicts a particular value for the power law exponent (as that in Eqns. 10 and 13). Hence, an observed power law scaling between the X-ray properties different from that predicted above does not imply the self-similar scenario, even though a power law relation is self-similar in a mathematical sense.

A very useful quantity to describe the ICM is the entropy S : it determines the structure of the ICM in galaxy clusters, together with the profile of the potential well. The low entropy gas sinks while the high entropy gas floats; hence the gas will convect until the iso-entropic surfaces will coincide with the equipotential surfaces of the dark matter potential (Voit 2005). This naturally leads to a state of hydrodynamical equilibrium, which is just an expression of its underlying entropy and potential profiles. Furthermore, since entropy can only increase, if we consider the cluster as a closed system within a certain radius, it retains the memory of the thermodynamical history of the intracluster gas.

The entropy S is defined as³

$$S = \frac{k_B T_{\text{gas}}}{(n_e)^{2/3}}. \quad (14)$$

Therefore, the scaling laws described above imply that the entropy parameter scales as

$$S \propto T_{\text{gas}} \propto M_{\text{tot}}^{2/3} \quad (15)$$

for purely gravitational heating.

These results can be combined to obtain other scaling relations and we list the most popular ones. In doing so, it is convenient to combine the dependence on cosmology and redshift in the factor $F_z = E_z \times (\Delta_z/\Delta_{z=0})^{1/2}$:

$$\begin{aligned} L_X &\propto F_z T_{\text{gas}}^2 \\ L_X &\propto F_z^{7/3} M_{\text{tot}}^{4/3} \\ L_X &\propto F_z^{9/5} Y_X^{4/5} \\ M_{\text{tot}} &\propto F_z^{-1} T_{\text{gas}}^{3/2} \\ M_{\text{tot}} &\propto F_z^{-2/5} Y_X^{3/5} \\ M_{\text{gas}} &\propto F_z^{-1} T_{\text{gas}}^{3/2} \\ S &\propto F_z^{-4/3} T_{\text{gas}} \end{aligned} \quad (16)$$

It should be stressed these equations are valid only if the condition of hydrostatic equilibrium holds. This is true only in the central part of the clusters, which is the most evolved one, while in the outskirts both the assumptions of thermal (e.g. Fox & Loeb 1997) and hydrostatic equilibrium (e.g. Nagai et al. 2007) brake down (for a review

³ The definition of entropy used in astrophysics of galaxy clusters is different from the classic thermodynamical entropy s , but the two are related through $s = k_B S + \text{constant}$ (Voit 2005).

on the physical processes occurring in the clusters outskirts see Reiprich et al. (2013) in this volume). This assumption also breaks down in disturbed systems undergoing mergers (Poole et al. 2007). Also, the very central core of a galaxy cluster can be out of equilibrium when there is AGN activity. Therefore one has to take care when interpreting the cluster profiles at both small and large radii and for unrelaxed systems using equations that rely on the assumptions of hydrostatic and thermal equilibrium.

Furthermore these simple analytic scaling relations employing F_z implicitly assume that clusters formed only recently. The validity of this assumption was examined in Böhringer et al. (2012) who compared scaling relations obtained from the results from N-body simulations. They find that modifications are needed, especially for relations that involve the gas density or gas mass. Böhringer et al. (2012) also provide a comprehensive comparison of their modified scaling relations to a number of observational studies. Here we limit the comparison to a number of recent studies and list constraints on the various scaling relations in Table 1. Some of the relations agree fairly well with the predictions from the self-similar model, whereas others show significant deviations.

2.2 Observations and deviation from self-similarity

2.2.1 The $L_X - T$ and $S - T$ scaling relation

Among the X-ray scaling relations, the first one to be studied was the $L_X - T$ relation, and it remains the best studied one (e.g. Mitchell et al. 1977, 1979; Mushotzky 1984; Edge & Stewart 1991; David et al. 1993; Markevitch 1998; Allen et al. 2001; Ikebe et al. 2002; Ettori et al. 2004a; Pratt et al. 2009; Mittal et al. 2011; Maughan et al. 2012). This is not surprising, since both quantities can be measured easily and almost independently from X-ray data. The gas temperature is determined from X-ray spectroscopic data while the luminosity is obtained from by integrating the surface brightness profile of the cluster from X-ray imaging data.

Several independent observational studies have shown that the $L_X - T$ relation does not scale self-similarly, as it would do if the heating is mostly due to gravitational processes (i.e. adiabatic compression during the infall and shock heating from supersonic accretion). Already from the earliest X-ray observations of galaxy clusters performed with ASCA, EXOSAT and ROSAT there has been a general consensus that the slope of the $L_X - T$ relation is significantly steeper, with a slope for the bolometric luminosity closer to 3 than to the theoretically predicted exponent of 2 (e.g. Mushotzky 1984; Edge & Stewart 1991; Markevitch 1998). Further studies with samples of lower mass galaxy groups assessed that the deviation from the self-similar scaling becomes larger below $kT \sim 3.5$ keV, marking a clear transition between galaxy groups and clusters (Ponman et al. 1996; Balogh et al. 1999; Maughan et al. 2012).

Figure 3 (*top panel*) shows a compilation of recent data for the $L_X - T$ relation. Table 1 lists the best fit slopes from a number of studies. The best fitting relations obtained for the samples with $T > 4$ keV (red line) and $T < 4$ keV (blue line) are also shown separately in Figure 3. Indeed the two subsamples do not share the same best fit solution.

Much effort has been spent over the last decade to determine the processes responsible for the deviation from self-similarity. These studies are now possible because samples of low mass systems are becoming available. Because of their fainter X-ray luminosity, galaxy groups require very deep observations, and this has limited the

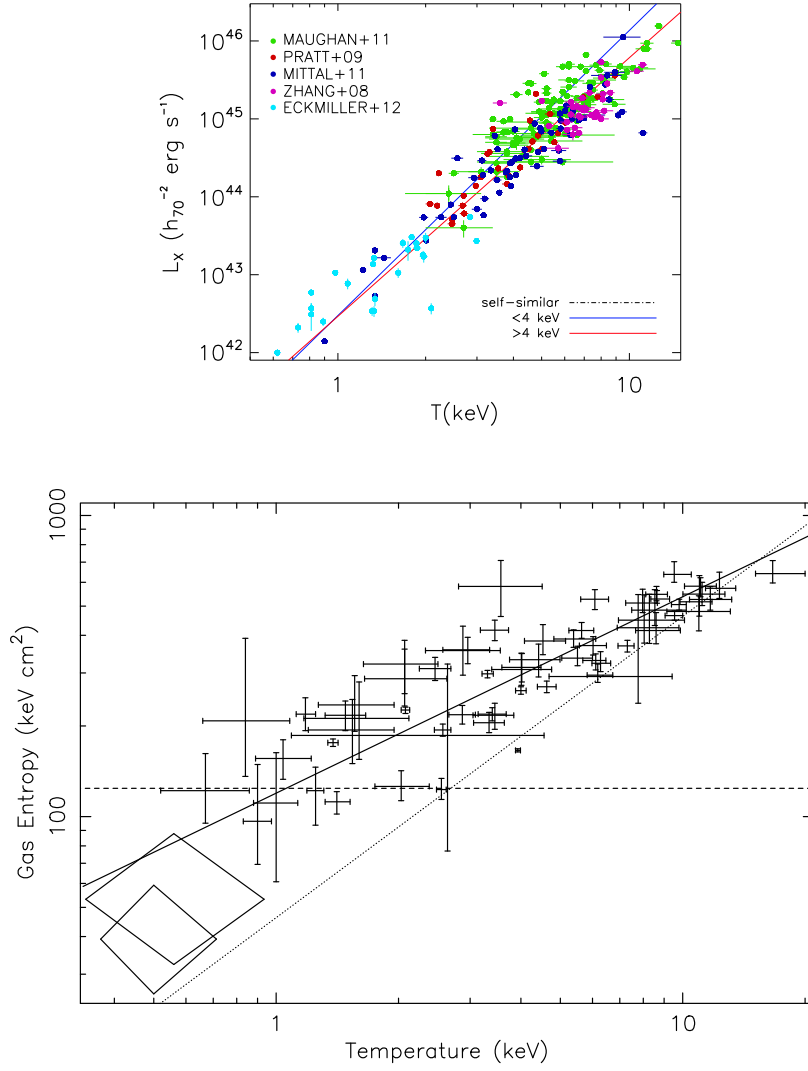


Fig. 3 *Top Panel:* Recent measurements of the $L_X - T$ relation for different samples of groups and clusters. Cyan circles mark measurements from the groups sample from Eckmiller et al. (2011), green circles from Maughan et al. (2012). Blue circles show the HIFLUGCS massive clusters (Mittal et al. 2011), red circles mark the REXCESS clusters (Pratt et al. 2009) and pink circles are LoCuSS clusters (Zhang et al. 2008). All the parameters are calculated at R_{500} . *Bottom panel:* Gas entropy versus temperature measured for a sample of galaxy groups and clusters. Observations suggest that gas entropy varies with the mean temperature to the power $2/3$ (solid line), a scaling which is at odds with the self-similar expectation (dotted line). The flattening of the relationship is likely due to the action of non-gravitational heating/cooling sources that has a greater impact on the least massive systems. (Figure from Ponman et al. 2003)

number of systems that have been observed. In the last few years deep X-ray surveys have provided the first statistically significant samples of X-ray galaxy groups (e.g. Finoguenov et al. 2007; Gastaldello et al. 2007; Sun et al. 2009; Eckmiller et al. 2011). For example Pratt et al. (2009) examined possible causes for the observed steeper slopes, concluding that it is mostly associated with the variation of the gas content with mass, while structural variations play only a minor role. There is currently a general consensus that the fraction of gas decreases as the mass decreases (Vikhlinin et al. 2006; Gastaldello et al. 2007; Pratt et al. 2009; Dai et al. 2010)⁴. As L_X is proportional to the square of the gas fraction, a change in the gas content of low mass systems (and as a function of radius) would lead to a reduction in the observed luminosity and consequently to a steepening of the relations. Complications to this very simple reasoning can be added by the increased importance of line emission from metals at low temperatures, which implies that the assumption of pure bremsstrahlung is not fulfilled, resulting in a different dependence of the luminosity on f_{gas} .

The deviation of the $L_X - T$ relation from the pure gravitational prediction can also be interpreted in terms of entropy variation (Evrard & Henry 1991; Bower 1997; Tozzi & Norman 2001; Borgani et al. 2001; Voit et al. 2002; Younger & Bryan 2007; Eckmiller et al. 2011). One way to inhibit the gas from reaching the center of the potential well, thus changing the gas fraction, is to increase the entropy of the gas. This implies the existence of an "entropy floor" for low mass systems that would make the gas more resistive to compression. Observations show that the cores of galaxy groups exhibit entropy in excess to that achievable by pure gravitational collapse (Ponman et al. 1999). Consequently, the scaling relation between entropy and temperature is flatter than predicted (Ponman et al. 2003, see bottom panel of Fig. 3). Furthermore observations of clusters at larger radii showed that the excess entropy increases by up to factor of 4 in the outskirts of galaxy clusters (Finoguenov et al. 2002). See Reiprich et al. (2013) for a summary of recent entropy observations in cluster outskirts.

The key to understanding the deviation from self-similarity is to know which processes regulate the increase of the entropy in galaxy clusters and groups. A boost in entropy can be induced either by heating the gas or by selectively removing gas with low entropy (i.e. lowering the gas density). This can only be achieved through non-gravitational processes such as radiative cooling, AGN feedback, star formation or galactic winds. These will affect low mass groups more strongly because of the lower gravitational binding energy for the gas. Furthermore, if feedback processes are triggered by galaxies, the combined mass of the member galaxies in groups is at least equal to that of the gas (Giodini et al. 2009) making the ratio source/recipient of excess entropy just about unbalanced.

The ICM heating can be due to processes internal to the clusters, such as late stellar or AGN heating coming mostly from the central galaxy, or due to pre-heating, i.e. prior to the cluster infall. In the last ten years studies have focused on understanding which processes contribute most during the thermodynamical history of the ICM. Pratt et al. (2010) examined the entropy profiles for clusters in the REXCESS sample, revealing that the scaling of gas entropy is shallower than self-similar in the inner regions, but that it steepens with radius, becoming consistent with the self-similar prediction at R_{500} . They argue that variations of the gas content with mass and radius are at the root of the observed departures from self-similarity of cluster entropy profiles and that results are consistent with a central heating source. The variation in the gas fraction

⁴ We note that Juett et al. (2010) claims this may be a selection effect.

within R_{500} as a function of the cluster mass was quantified by Pratt et al. (2009). The results are consistent with a scenario in which AGN feedback combined with merger mixing maintains an elevated central entropy level in the majority of the clusters. Similar conclusions were reached by Maughan et al. (2012) using a sample of 114 clusters observed with XMM. They pointed out, however, that the most massive cool core systems follow the self similar $L_X - T$ scaling relation (when the core is excluded) and do not exhibit a central entropy excess. Non-cool core systems, on the other hand, being dynamically unrelaxed, would never follow self-similar scaling relations because merger shocks enhance the entropy input. Further evidence supporting central heating has also been found by Mantz et al. (2010a) and Mittal et al. (2011).

The $L_X - T$ relation shows a large scatter about the mean of $\sigma \sim 0.7$ dex (Pratt et al. 2009). Using high-resolution imaging it has now become clear that this scatter reflects the prevalence in a mass limited sample of clusters exhibiting a boost in the X-ray surface brightness in their inner 50-100 kpc. Because of the corresponding temperature drop in this region, these systems have been dubbed ‘cool cores’, and they are associated with the inflow of gas from the external regions of the clusters towards the core.

For a given mass, cool-core clusters are generally more X-ray luminous than non-cool-cores. As a result they are common in X-ray selected samples. Since most of the luminosity in cool-cores comes from the central region of the cluster, the scatter in the $L_X - T$ is strongly reduced (to roughly half) when the X-ray luminosity is estimated outside the core of the cluster (Markevitch 1998; Pratt et al. 2009; Mittal et al. 2011; Maughan et al. 2012). Another source of scatter in the $L_X - T$ relation is caused by morphologically disturbed systems where the assumptions of hydrodynamic equilibrium and the spherical symmetry are invalid, biasing the estimate of the luminosity (e.g. Maughan et al. 2012).

2.3 The $M_{\text{tot}} - T$ relation

The total mass-temperature relation ($M_{\text{tot}} - T$) is another important source of information about the cluster physics, because it provides the link between the properties of the hot gas in the ICM and the overall mass: in the absence of strong cooling, the temperature of a cluster is T is only determined by the depth of its potential well.

There are two approaches to determine the $M_{\text{tot}} - T$ relation with an X-ray survey. The first is to study a small sample of clusters for which the assumptions required to determine its total mass can be trusted with a high level of confidence (e.g. a massive relaxed systems). Unfortunately such a limited sample may not be representative of the cluster population as a whole. Alternatively, a large sample can be used, but the usual assumption of hydrostatic equilibrium may be invalid for some of the clusters, introducing additional scatter in the measured relation. However, since the link between the ICM temperature and the total mass is determined only by the condition of hydrostatic equilibrium, the $M_{\text{tot}} - T$ relation should have a small scatter because it is less sensitive to processes of heating and cooling. As before, any deviations from self-similarity would indicate that other physical processes are at play in addition to gravity.

Böhringer et al. (2012) have summarized observational constraints from the literature (also see our compilation in Table 1) The general consensus is that slope of the $M_{\text{tot}} - T$ relation is self-similar for massive clusters (e.g. Finoguenov et al. 2001; Arnaud et al. 2005; Vikhlinin et al. 2009a). When low mass systems are considered, the

best fit slope is slightly steeper than the self similar prediction (the values range from 1.5–1.7; e.g. Arnaud et al. 2005; Sun et al. 2009; Eckmiller et al. 2011). The $M - T$ relation seems to be fairly robust against deviations from self-similarity. Furthermore, the scatter in the measured $M_{\text{tot}} - T$ relation is considerably smaller than that of the $L_X - T$ relation (15%, Mantz et al. 2010a), making it very attractive for its use in cosmological studies with galaxy clusters.

It is important to understand the nature of the scatter in this relation since the current uncertainty on the determination of the cosmological parameters Ω_m and w from X-ray studies of clusters is dominated by uncertainties in the mass-observable relation, as shown by Cunha & Evrard (2010). For instance, underestimating the scatter in the $M_{\text{tot}} - T$ relation can lead to an overestimate of σ_8 (Randall et al. 2002). An added concern is that the assumption of hydrostatic equilibrium is incorrect.

Simulations have also shown that the intrinsic scatter in the $M_{\text{tot}} - T$ relation is associated with the presence of substructure (O’Hara et al. 2006; Yang et al. 2009). Substructure is mostly associated with merging systems, where the mass measurement will be biased because the assumptions of hydrostatic equilibrium and spherical symmetry are invalid. This will result in systematically underestimated masses up to 20% as shown in numerical simulations (Evrard 1990; Evrard et al. 1996; Rasia et al. 2006; Nagai et al. 2007; Shaw et al. 2010; Rasia et al. 2012) and observations (Mahdavi et al. 2008, 2012). Additional sources of scatter are likely present, as discussed in Poole et al. (2007) who showed that the increase in the dispersion due to mergers it is not enough to account for all the scatter in the $M_{\text{tot}} - T$ relation.

2.4 $M_{\text{tot}} - Y_X$ and $M_{\text{tot}} - M_{\text{gas}}$ relation

Kravtsov et al. (2006) proposed the use of the X-ray equivalent of the SZ signal (see §4 for details), defined as

$$Y_X = M_{\text{gas}} \times T. \quad (17)$$

This quantity is related to the total thermal energy of the ICM and it appears to be a low scatter mass indicator. The use of this quantity has been motivated by results from hydrodynamic numerical simulations, which showed that the temperature deviations from the $M_{\text{tot}} - T$ relation are anti-correlated with the residuals in M_{gas} from the $M_{\text{tot}} - M_{\text{gas}}$ relation. This anti-correlation tends to suppress the scatter in the $M_{\text{tot}} - Y_X$ relation (down to 5-7% for $M_{500} - Y_X$) independently of the dynamical state of the objects. Whether or not Y_X is the lowest scatter estimator in simulations is a matter of debate. For instance, Stanek et al. (2010) used an SPH code, and found a positive correlation between temperature and gas-mass deviations, thus contradicting the result by Kravtsov et al. (2006),

X-ray observations have shown that the measured $M_{\text{tot}} - Y_X$ relation agrees with the self similar prediction from the simulations (Arnaud et al. 2007; Maughan 2007; Zhang et al. 2008; Vikhlinin et al. 2009a), albeit with an offset in the normalization. This could be due to an underestimate of the gas fraction in simulations or due to deviations from hydrostatic equilibrium (Arnaud et al. 2007). Figure 4 (*left panel*) shows the $M_{\text{tot}} - Y_X$ relation from Arnaud et al. (2007) and the comparison with the predictions from numerical simulations. Recent observational studies (Juett et al. 2010; Okabe et al. 2010; Mahdavi et al. 2012) found a larger scatter of this relation (up to

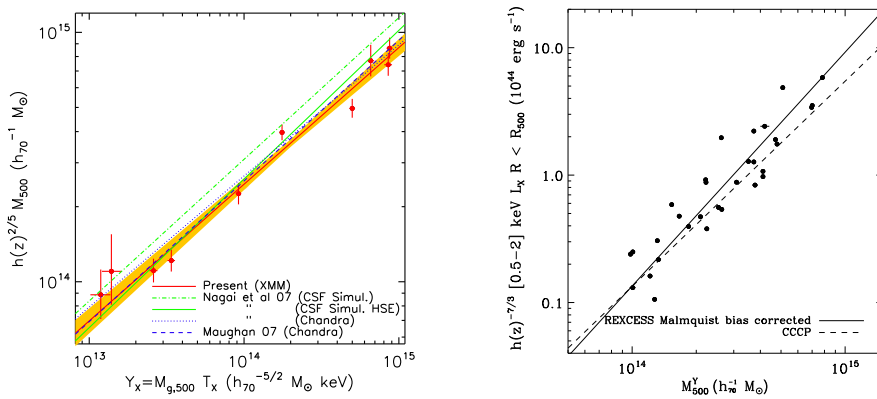


Fig. 4 *left*: $E_z^{2/5} M_{\text{tot}} - Y_X$ relation for a sample of 10 local relaxed clusters observed with XMM compared with the predicted relations from numerical simulations and the observed one with Chandra. (Figure from Arnaud et al. 2007). *right*: Comparison between the Malmquist bias corrected $L_X(0.5 - 2 \text{ keV}) - M_Y$ relations obtained by Pratt et al. (2009) and Vikhlinin et al. (2009a). The points are the bias-corrected REXCESS values. Figure from Pratt et al. 2009.

$\sim 20\%$ against $< 10\%$ in the simulations). Interestingly, Mahdavi et al. (2012) find that the scatter in the $M_{\text{tot}} - Y_X$ relation is the same for clusters with low and high central entropies, suggesting that Y_X may be well suited as a proxy for large cluster surveys.

Interestingly, M_{gas} appears to have a very small scatter with the cluster total mass, with only a mild dependence with redshift (e.g. Vikhlinin et al. 2003). Comparing to weak lensing observations both Okabe et al. (2010) and Mahdavi et al. (2012) argue that M_{gas} is the lowest scatter mass proxy. Mahdavi et al. (2012) found that the scatter for clusters with low central entropies is particularly low, suggesting that the gas fractions vary very little for such clusters. Zhang et al. (2008) found a lower gas mass in low mass systems than expected from a purely gravitational scenario, implying a steepening with respect to the prediction of the self-similar scenario.

2.5 $L_X - M_{\text{tot}}$ relation

Future all-sky X-ray surveys, such as eROSITA, will image hundreds of thousands of clusters with very shallow observations, collecting too few photons to extract spectra or mass profiles. On the other hand a measure of the X-ray luminosity will be always possible if redshift information is available. Hence the correlation between the X-ray luminosity and total mass is an important tool for cosmology because it correlates the total mass of a system with its ‘cheapest’ X-ray observable. This does, however, require a very accurate determination of the $L_X - M_{\text{tot}}$ relation and its scatter.

If a large range in mass is covered, the degeneracy between Ω_m and σ_8 can be broken (Reiprich & Böhringer 2002). Hence the calibration of this relation needs to be extended to low mass groups. A large number of observations (e.g. Reiprich & Böhringer 2002; Ettori et al. 2002; Maughan et al. 2006; Maughan 2007; Chen et al. 2007; Vikhlinin et al. 2009a; Pratt et al. 2009; Arnaud et al. 2010; Mantz et al. 2010a; Eckmiller et al. 2011; Reichert et al. 2011) show that the X-ray luminosity is heavily affected by non-gravitational processes. Observed slopes for the $L_X - M_{\text{tot}}$ relation are $\sim 1.4-1.9$, steeper than the

Table 1 Overview of the most recent published scaling relations.

relation	observed	predicted	comments	reference	Note
$L_X - T$	$2.26 \pm 0.29^\dagger$		50 clusters, $z = 0.15 - 0.55$	Mahdavi et al. 2012	<i>a, d, e</i>
	$2.25 \pm 0.21^\ddagger$		26 clusters, $z = 0.01 - 0.05$	Eckmiller et al. 2011	<i>c, d, e, f</i>
	$2.64 \pm 0.20^\ddagger$		64 clusters, $z = 0.01 - 0.15$	Mittal et al. 2011	<i>a, e, h</i>
	$2.53 \pm 0.15^\parallel$		232 clusters, $z = 0.04 - 1.46$	Reichert et al. 2011	<i>a</i>
	$2.72 \pm 0.18^\uparrow$	2	114 clusters, $z = 0.10 - 1.30$	Maughan et al. 2012	<i>a, d, e</i>
	$2.70 \pm 0.24^\parallel$		31 clusters, $z = 0.06 - 0.17$	Pratt et al. 2009	<i>a</i>
	$3.35 \pm 0.32^\uparrow$		31 clusters, $z = 0.06 - 0.17$	Pratt et al. 2009	<i>a</i>
	$2.78 \pm 0.13^\parallel$		31 clusters, $z = 0.06 - 0.17$	Pratt et al. 2009	<i>a, d, e</i>
	$2.61 \pm 0.32^\downarrow$		37 clusters, $z = 0.14 - 0.30$	Zhang et al. 2008	<i>a, e</i>
$M_{\text{tot}} - T$	$1.68 \pm 0.20^\ddagger$		26 clusters, $z = 0.01 - 0.05$	Eckmiller et al. 2011	<i>e, f</i>
	$1.76 \pm 0.08^\ddagger$	1.5	232 clusters, $z = 0.04 - 1.46$	Reichert et al. 2011	
	$1.53 \pm 0.08^\ddagger$		17 clusters, $z = 0.03 - 0.05$	Vikhlinin et al. 2009a	<i>e</i>
	$1.65 \pm 0.04^\uparrow$		43 clusters, $z = 0.01 - 0.12$	Sun et al. 2009	<i>f</i>
	$1.65 \pm 0.26^\downarrow$		37 clusters, $z = 0.14 - 0.30$	Zhang et al. 2008	<i>e</i>
$L_X - M_{\text{tot}}$	$1.34 \pm 0.18^\ddagger$		26 clusters, $z = 0.01 - 0.05$	Eckmiller et al. 2011	<i>c, d, f</i>
	$1.51 \pm 0.09^\parallel$		232 clusters, $z = 0.04 - 1.46$	Reichert et al. 2011	<i>a</i>
	$1.76 \pm 0.13^\uparrow$		31 clusters, $z = 0.06 - 0.17$	Arnaud et al. 2010	<i>c, g</i>
	$1.64 \pm 0.12^\uparrow$		31 clusters, $z = 0.06 - 0.17$	Arnaud et al. 2010	<i>c</i>
	$1.90 \pm 0.11^\parallel$	1.3	31 clusters, $z = 0.06 - 0.17$	Pratt et al. 2009	<i>a, g</i>
	$1.62 \pm 0.11^\parallel$		31 clusters, $z = 0.06 - 0.17$	Pratt et al. 2009	<i>c, g</i>
	$1.83 \pm 0.14^\uparrow$		31 clusters, $z = 0.06 - 0.17$	Pratt et al. 2009	<i>c, g</i>
	$1.53 \pm 0.10^\parallel$		31 clusters, $z = 0.06 - 0.17$	Pratt et al. 2009	<i>c, d</i>
	$1.71 \pm 0.12^\uparrow$		31 clusters, $z = 0.06 - 0.17$	Pratt et al. 2009	<i>c, d</i>
	$1.61 \pm 0.14^\ddagger$		17 clusters, $z = 0.03 - 0.05$	Vikhlinin et al. 2009	<i>b</i>
	$2.33 \pm 0.70^\downarrow$		37 clusters, $z = 0.14 - 0.30$	Zhang et al. 2008	<i>a</i>
$M_{\text{gas}} - M_{\text{WL}}$	$1.04 \pm 0.10^\dagger$	1	50 clusters, $z = 0.15 - 0.55$	Mahdavi et al. 2012	<i>i</i>
$M_{\text{WL}} - Y_X$	$0.56 \pm 0.08^\dagger$	0.6	50 clusters, $z = 0.15 - 0.55$	Mahdavi et al. 2012	<i>i</i>
$M_{\text{tot}} - Y_X$	$0.53 \pm 0.06^\ddagger$	0.6	26 clusters, $z = 0.01 - 0.05$	Eckmiller et al. 2011	<i>e, f</i>
$M_{\text{tot}} - Y_X$	$0.57 \pm 0.03^\ddagger$	0.6	17 clusters, $z = 0.03 - 0.05$	Vikhlinin et al. 2009	<i>e</i>
$M_{\text{tot}} - Y_X$	$0.57 \pm 0.01^\uparrow$	0.6	43 clusters, $z = 0.01 - 0.12$	Sun et al. 2009	<i>f</i>
$S - T$	$0.92 \pm 0.24^\uparrow$	1	31 clusters, $z = 0.06 - 0.17$	Pratt et al. 2010	
$L_X - Y_X$	$1.07 \pm 0.08^\uparrow$	0.8	31 clusters, $z = 0.06 - 0.17$	Arnaud et al. 2010	<i>c, g</i>
$L_X - Y_X$	$0.82 \pm 0.03^\parallel$	0.8	31 clusters, $z = 0.06 - 0.17$	Pratt et al. 2009	<i>c, d, e</i>
$M_{\text{gas}} - T$	$2.12 \pm 0.12^\uparrow$	1.5	31 clusters, $z = 0.06 - 0.17$	Croston et al. 2008	
$M_{\text{gas}} - T$	1.99 ± 0.11^b	1.5	31 clusters, $z = 0.06 - 0.17$	Croston et al. 2008	
$M_{\text{gas}} - T$	$1.86 \pm 0.19^\downarrow$	1.5	37 clusters, $z = 0.14 - 0.30$	Zhang et al. 2008	<i>e</i>

^a bolometric luminosity.

^b luminosity in the 0.5-2 keV band.

^c luminosity in the 0.1-2.4 keV band.

^d core excised luminosity.

^e core excised temperature.

^f limited to systems with temperature ≤ 3 keV.

^g corrected for Malmquist bias.

^h individual Malmquist bias corrections for SCC, WCC and NCC clusters.

ⁱ weak lensing mass.

[†] bayesian method by Hogg et al. (2010).

[‡] BCES (Akritas & Bershady 1996) bisector.

[↑] BCES orthogonal.

[∥] BCES $Y|X$.

[↓] BCES $X|Y$.

[↓] ODRPACK orthogonal.

^b WLSS.

self-similar prediction of 4/3. Furthermore, both the slope and normalization of this relation can vary quite significantly depending on the energy band⁵ and method used for the flux extraction. In Figure 4 (*right panel*) we compare the $L_X - M_{\text{tot}}$ relation derived by Pratt et al. (2009) to the results from Vikhlinin et al. (2009a). There is a general agreement for the recovered slopes and normalizations between measurements.

Among the various X-ray scaling relations the scatter of $\sim 40\%$ in the $L_X - M_{\text{tot}}$ relation is the largest. This has been attributed to the presence of cool-cores and the overall dynamical state of clusters. Most of the scatter derives from the central part of the cluster (within $\sim 0.1-0.2$ Mpc) where cooling and merging effects are most pronounced. Excluding the cluster core can reduce the scatter to less than 10% in mass (Markevitch 1998; Mantz et al. 2010a).

In an attempt to reduce the scatter between the mass proxies and the total cluster mass, Ettori et al. (2012) introduced a generalized scaling law, defined as

$$M_{\text{tot}} = 10^K A^a B^b. \quad (18)$$

They found a locus of minimum scatter that relates the logarithmic slopes of two generalized independent variables, namely the temperature T , which traces the depth of the cluster potential, and another one accounting for the gas density distribution, such as gas mass M_{gas} or X-ray luminosity. This minimum scatter locus corresponds to the plane where L_X : $b_M = -3/2a_M + 3/2$ and $b_L = -2a_L + 3/2$ for $A = M_{\text{gas}}$ and L_X , respectively, and $B = T$. Within this approach, all the known scaling relations appear as particular realizations of generalized scaling relations. A new relation is also introduced, $M_{\text{tot}} \propto (L_X T)^{1/2}$, which is analogous to the $M_{\text{tot}} - Y_X$ relation, once luminosity is used instead of gas mass. Although, this approach is still affected by mass calibration and selection effects, it allows a minimization of the scatter imposing a new constraint on the slope of the scaling laws.

3 Evolution

The X-ray scaling relations are expected to be redshift-dependent, even in the simplest case where gravity dominates. This is because of the cosmological expansion and the corresponding evolution of the background matter density of the Universe. The evolution is expected to be stronger when non-gravitational processes are considered, due to the growing relative importance of such processes to the energy budget of galaxy clusters as a function of redshift (e.g. the AGN luminosity function evolves strongly with redshift in both X-ray and radio bands).

In the self-similar scenario, the scale (in mass or T) does not play any role (i.e. groups and clusters are the same kind of objects) and as a result only the normalization depends on cosmic time/redshift. This dependence is generally parametrized by the relative change in the Hubble parameter E_z (or F_z) and one can write a scaling relation between quantities X and Y as:

$$Y(X, z) = X_0 \times E(z)^\beta X^\alpha. \quad (19)$$

⁵ Apart from the bolometric value which requires an extrapolation, the luminosity is often derived using the 0.1-2.4 or 0.5-2 keV bands.

One can consider more complicated scenarios in which the slope also depends on redshift, although this would require some additional physics. At the moment, however, the paucity of well defined samples at high redshift (and the narrow range in mass surveyed as a good sample of galaxy groups at high- z is lacking) strongly limits the present constraints on the redshift evolution of the scaling relations or any clear detection of departure from the self-similar predictions.

Understanding the evolution of the scaling relations is nonetheless crucial in order to use clusters for cosmology, especially for the determination of the evolution of the mass function with redshift. While the mass-observable scaling relations are calibrated reasonably well at low redshift, at least for relaxed clusters, measuring these relations at high redshift is considerably more challenging, due to the long observations required to obtain sufficiently deep X-ray data to constrain the cluster properties. For this reason no clear consensus has been reached on the evolution of the X-ray scaling relations, despite a number of observational studies carried out in the past decade (e.g. Vikhlinin et al. 2002, 2009a; Ettori et al. 2004b; Kotov & Vikhlinin 2005; Maughan et al. 2006; Maughan 2007; Maughan et al. 2012; O’Hara et al. 2006; Morandi et al. 2007; Branchesi et al. 2007; Pacaud et al. 2007; Andreon et al. 2011; Reichert et al. 2011).

For example Ettori et al. (2004b) (see top panel of Fig. 5), O’Hara et al. (2006) and Reichert et al. (2011) found a negative evolution for the $L_X - T$ relation, at odds with the result by Kotov & Vikhlinin (2005) who observed a positive evolution, and Pacaud et al. (2007) who found no significant evolution. In general, all the relations involving parameters that depend on the gas density show significant deviations from the predictions; a clear indication that non-gravitational processes cannot be neglected. In contrast, the $M_{\text{tot}} - T$ relation is generally very close to the self-similar prediction (see bottom panel of Fig. 5), which is not surprising because it mostly depends on the dark matter potential. A compilation of the most recent publications and their main results can be found in Reichert et al. (2011).

There are several reasons why the results from different studies appear to be contradictory. One of the main problems in achieving a consensus is the difficulty in accounting for selection biases caused by the lack of concordance between different studies in the cluster selection. The use of miscellaneous archival cluster samples leads to selection bias corrections that may vary from sample to sample and alter the measured evolution especially when considering the poor statistics due to the small sample size. Since clusters do not have a clear outer boundary (see Reiprich et al. 2013, for a review on the cluster outskirts) the different choices of defining the fiducial radius (e.g. redshift-independent or not) within which the cluster properties are considered, may also play a role, although Reichert et al. (2011) found that this effect should be negligible. Importantly, the assumed local scaling relation which is the reference to compare the high-redshift data to, has a direct impact on the inferred evolution. This is likely to introduce systematic errors. As shown in the previous sections, the luminosity is sensitive to the central gas density such that tighter scaling relations involving the X-ray luminosity are obtained by excising the core. The lack of photon collecting power of current instruments makes the cool cores excision problematic at high redshift and increases the scatter in the scaling relations making it difficult to disentangle the evolution from the no-evolution scenario.

Major progress will come from X-ray observations that measure the thermodynamical properties of high redshift clusters. Among these are the XMM Deep Cluster Project (XDGP2; Fassbender et al. 2011) that has so far spectroscopically confirmed

22 clusters at $z > 0.8$. The study of these high redshift objects is extremely important. Although massive clusters are rare at any redshift, they are most sensitive to cosmology, allowing a more precise study of the evolution.

As discussed in more detail in §6, the expected evolution of mass-observable scaling relations has also been studied using samples extracted from large cosmological hydrodynamical simulations. The predictions depend on the adopted prescriptions for cooling and feedback. Hence observational constraints have the potential to constrain the non-gravitational physics. However, Short et al. (2010) point out that a statistically meaningful comparison with observations is impossible at the moment, because the largest samples of high-redshift clusters currently available are still affected by strong selection biases.

4 SZ scaling relations

The thermal Sunyaev-Zeldovich effect (SZE) is a distortion of the black body spectrum of the photons from the cosmic microwave background (CMB) in the direction of galaxy clusters. As first predicted by Sunyaev & Zeldovich (1970, 1972), the low-energy CMB photons can interact via inverse Compton scattering with the free electrons in the intra-cluster medium. This scattering causes a small change of the mean photon energy as

$$\frac{\Delta\nu}{\nu} \simeq \left(\frac{kT}{m_e c^2} \right) \sim 10^{-2}, \quad (20)$$

where m_e is the mass of the electron. The frequency shift causes an increase in the CMB intensity in the high frequency (Wien) part of the spectrum and a decrement in the Rayleigh-Jeans tail. This corresponds to a brightness fluctuation in the CMB of $\sim 10^{-4}$, which is roughly an order of magnitude larger than the cosmological signal from the primary anisotropies.

Figure 6 plots the difference in intensity between the on-cluster distorted spectrum and the off-cluster black-body spectrum for a massive cluster ($y=5 \times 10^{-4}$, where y is defined below). Within a non-relativistic Thomson diffusion limit⁶, the spectral shape for the SZ effect derives from the Kompaneets equation (Kompaneets 1957) and is defined analytically. Implementation of relativistic corrections due to the weakly relativistic tail of the electron velocity distribution leads to a weak dependence of this spectral shape with the electron gas temperature (e.g., Rephaeli 1995; Pointecouteau et al. 1998; Challinor & Lasenby 1999).

The magnitude of the decrement in the CMB is proportional to the line-of-sight integral of the product of gas density (n_e) and temperature (T_e)

$$\Delta y = -2yI_\nu, \quad (21)$$

where y is the Comptonization parameter, and is defined as

$$y = \frac{\sigma_T k_B}{m_e c^2} \int T_e n_e dl, \quad (22)$$

where k_B is the Boltzmann constant and σ_T is the Thompson cross-section. This equation corresponds to the integrated thermal pressure of the intra-cluster gas along the line of sight (since $P = n_e k_B T_e$ in the ideal gas approximation).

⁶ The non-relativistic approximation for the SZ effect roughly holds for clusters with ICM temperatures $kT \leq 10$ keV.

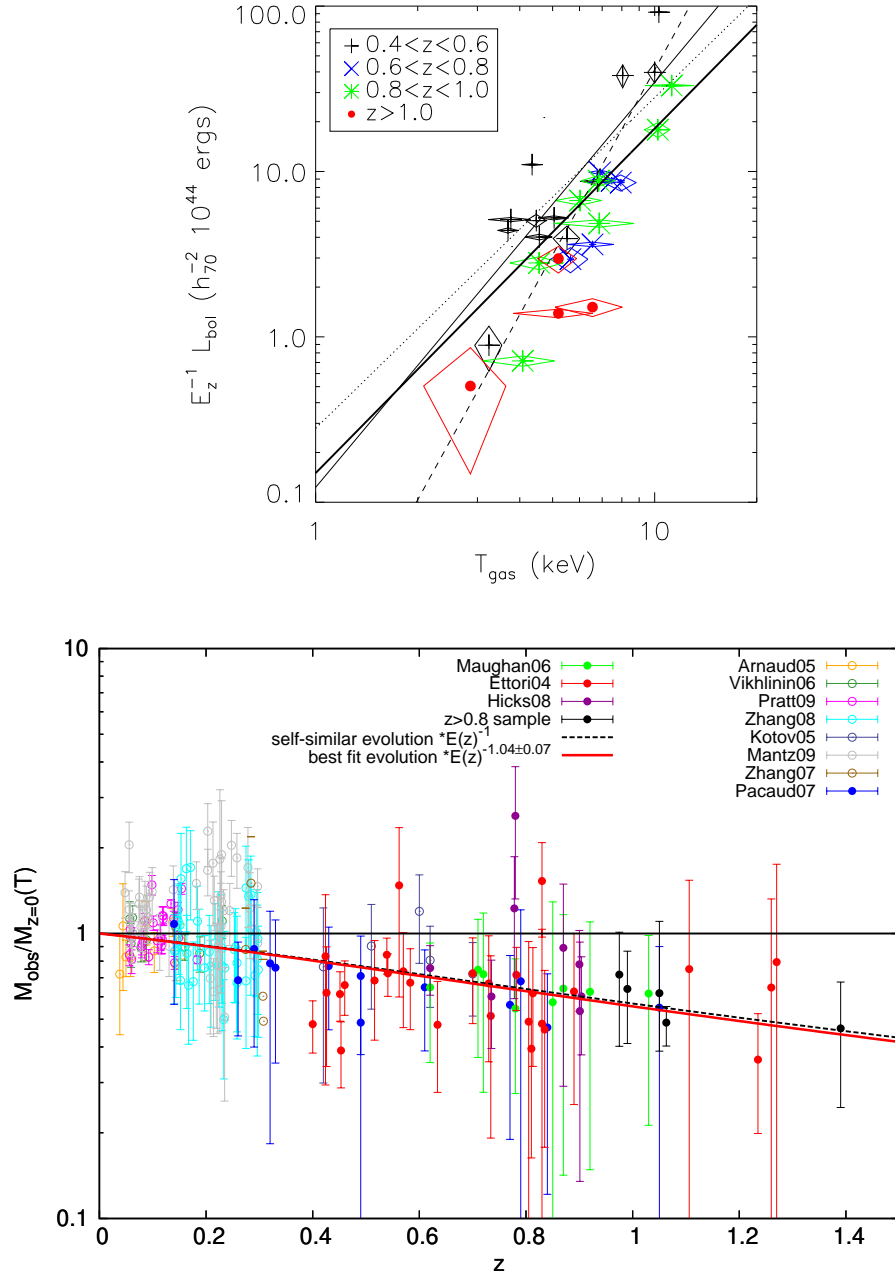


Fig. 5 *Upper Panel:* $E_z^{-1} L_X - T$ relation for a sample of 28 objects observed with Chandra in the z -range 0.4-1.3. Dotted line: slope fixed to the self-similar value. Dashed line: slope free. The solid lines represent the local best-fit results (from thinnest to thickest line): Markevitch (1998), Arnaud & Evrard (1999), Novicki et al. (2002). The evolution is evaluated by fitting the relation $\log Y = \alpha + A \log X + B \log(1+z)$ to the data, where (α, A) are the best-fit results obtained from a sample of objects observed at lower redshift. (Credit: Ettori et al., A&A, vol.417, pg.13, 2004, reproduced with permission © ESO). *Bottom Panel:* Redshift evolution of the $M_{\text{tot}} - T$ relation. Black-dashed line: self-similar prediction ($\propto E_z^{-1}$). Continuous red line: best-fit evolution ($\propto E_z^{-1.04 \pm 0.07}$). Credit: Reichert et al., A&A, vol.535, pg.A4, 2011, reproduced with permission © ESO.

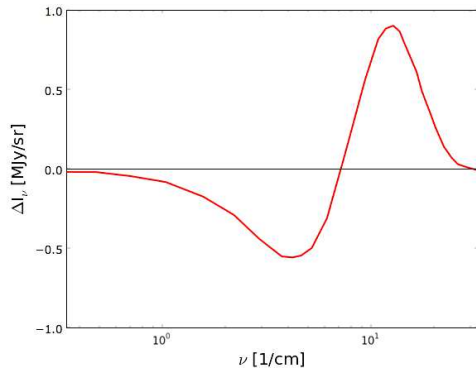


Fig. 6 Differences in intensity between the on-cluster distorted spectrum and the off-cluster black-body spectrum for a massive cluster with $y=5\times 10^{-4}$.

Being proportional to the integrated thermal pressure support within clusters, the magnitude of the SZ-effect is an ideal proxy for the mass of the gas in a galaxy cluster, M_{gas} , and thereby of the total mass, M_{tot} . This can be illustrated through the integrated Comptonization parameter defined as the integral of y over the solid angle under which the cluster is seen, i.e., Ω :

$$Y_{\text{SZ}} = \int_{\Omega} y d\Omega = \frac{1}{D_A^2} \frac{\sigma_T k_B}{m_e c^2} \int_V n_e T_e dV \quad (23)$$

where D_A is the angular distance to the cluster and V is the physical volume of the cluster. In the context of an isothermal model, Y_{SZ} is proportional to the integral of the electron density n_e over a cylindrical volume, which corresponds to the gas mass in the same volume. Assuming a gas fraction $f_{\text{gas}} = M_{\text{gas}}/M_{\text{tot}}$ we thus obtain

$$Y_{\text{SZ}} D_A^2 \propto T_e \int n_e dV = M_{\text{gas}} T_e = f_{\text{gas}} M_{\text{tot}} T_e. \quad (24)$$

Using Eqn. 24 in combination with the scaling $T_e \propto M_{\text{tot}}^{2/3} E(z)^{2/3}$, assuming hydrostatic equilibrium and an isothermal distribution for both the dark matter and the cluster gas (e.g Bryan & Norman 1998), we can obtain the following scaling relations for the integrated SZ signal and others observables:

$$\begin{aligned} Y_{\text{SZ}} D_A^2 &\propto f_{\text{gas}} T_e^{5/2} E(z)^{-1} \\ Y_{\text{SZ}} D_A^2 &\propto f_{\text{gas}} M_{\text{tot}}^{5/3} E(z)^{2/3} \\ Y_{\text{SZ}} D_A^2 &\propto f_{\text{gas}}^{-2/3} M_{\text{gas}}^{5/3} E(z)^{2/3} \end{aligned} \quad (25)$$

Equations 21 and 22 show that the amplitude of the SZ-effect is independent of redshift. Therefore, in contrast to X-ray and optical measurements, it does not undergo surface brightness dimming (i.e., $\propto (1+z)^{-4}$) since this is exactly compensated by the increase of the CMB intensity as $\propto (1+z)^4$ (at higher redshift we are probing a younger Universe where the CMB temperature is higher). It should be stressed that the actual SZ measurements are flux measurements; they are directly proportional to the integrated Compton parameter as expressed in Eqn. 23. Hence they do suffer from

a dimming; in the case of unresolved clusters this is determined by the ratio of the cluster solid angle over the instrumental beam.

The lack of a dependence with redshift and the direct proportionality to the total mass of the cluster should make SZ selected samples very close to mass limited. This makes the SZE an excellent probe for cluster cosmology. Large area SZ surveys carried out by large, single dish ground-based or space telescopes (such as SPT, ACT and *Planck*) are performing such studies and are delivering samples with significantly higher median redshifts compared to X-ray selected cluster catalogues (e.g., Reichardt et al. 2013).

The biggest challenge for blind SZ surveys is the extraction of the SZ signal and the separation between the fore- and background structures as well as the astrophysical signal. The diffuse gas that resides in large-scale filaments provides only a negligible contamination due to its comparatively low density and temperature. Small halos, on the other hand, are expected to be present in large number and cannot be resolved with the current SZ observations; they may provide a significant contamination as shown by White et al. (2002) using cosmological hydrodynamical simulations. The main signal contamination is expected to come from other astrophysical emissions such as infrared and radio point sources, cosmic infrared background fluctuations, Galactic emission and CMB contaminations (e.g., Aghanim et al. 2005). To optimally exploit large SZ samples in cosmological and astrophysical studies, well calibrated relations between the total mass and the SZ flux are required (e.g., da Silva 2004; Aghanim et al. 2009).

SZ and X-ray measurements naturally complement each other. In fact, due to the respective dependence on the gas density profile, i.e., n_e and n_e^2 respectively, density, temperature and therefore mass profiles can be inferred from joint SZ and X-ray analyses out to very large radii (e.g., Kitayama et al. 2004; Basu et al. 2010). Furthermore X-ray and SZ measurement can be combined to determine the Hubble parameter (H_0 ; Silk & White 1978) by measuring the distances to clusters.

The SZ effect as described here is usually called ‘thermal’ and largely dominates over the ‘kinetic’ SZ effect that is caused by the comoving bulk motion of the hot electrons in the intra-cluster medium (Sunyaev & Zeldovich 1980). The detection and quantification of the kinetic SZ effect is an ongoing topic of discussion (e.g., Atrio-Barandela et al. 2008; Kashlinsky et al. 2010; Hand et al. 2012). We refer to the reviews by Rephaeli (1995), Birkinshaw (1999) and Carlstrom et al. (2002) for a more detailed discussion of the SZE effect and related issues.

4.1 SZ scaling relations: pre-survey-era observations

The first significant detection of the thermal SZE was reported by Birkinshaw et al. (1978), only six years after the concept was proposed by Sunyaev & Zeldovich (1972). The history of successful targeted observations of clusters to detect the SZ effect goes back two decades, when pioneering observations were made with interferometers such as the Owen Valley Radio Observatory (OVRO; Birkinshaw et al. 1991, Herbig et al. 1995), the OVRO/BIMA interferometers (Carlstrom et al. 1996), or single dish bolometric instruments such as the Sunyaev-Zel’dovich Imaging Experiment (SuZIE; Holzapfel et al. 1997), the Diabolo photometer at the focus of the IRAM 30m radio telescope (Désert et al. 1998) and the NOBA instrument on the 45m NRO telescope (Komatsu et al. 1999).

In the last decade these measurements have been expanded to samples of clusters and the focus has moved to understanding the correlation between the SZ signal and other clusters observables, especially those related to the total mass. To this end a number of early studies targeted small samples of (well-)known clusters. Due to the intrinsic limitations of these SZ measurements, as well as the reach of the X-ray data, most of these studied were intrinsically limited to the inner regions of the clusters (e.g. Cooray 1999; McCarthy et al. 2003; Morandi et al. 2007). Benson et al. (2004) showed that the integrated SZ flux is a more robust observable than the central values of the SZ signal and found a strong correlation with X-ray temperature using a sample of 15 clusters obtained with SuZIE and X-ray temperatures from the ASCA experiment. More recently, Bonamente et al. (2008) examined the scaling relations between Y_{SZ} and total mass, gas mass and gas temperature using 38 clusters observed with *Chandra* and OVRO/BIMA and found that the slope and the evolution of the observed relations agree with that predicted by a self-similar model in which the evolution of cluster is dominated by gravitational processes (also see Huang et al. 2010, for a similar result using AMiBA).

Marrone et al. (2009) measured the relation between Y_{SZ} and lensing mass within 350 kpc, derived from a strong and weak lensing analysis of HST observations of 14 X-ray luminous clusters of galaxies. They found no evidence of segregation in Y between disturbed and undisturbed clusters, as had been seen with T_X on the same physical scales. This result confirmed that SZE may be less sensitive to the details of cluster physics in cluster cores compared to X-ray observations, as suggested by simulations. More recently, Marrone et al. (2012) studied a sample of 18 clusters using weak lensing. They found an intrinsic scatter of 20% in the weak lensing mass at fixed Y , with a suggestion of a dependence on morphology. Hoekstra et al. (2012) compared their weak lensing masses to results from Bonamente et al. (2008) and Planck Collaboration et al. (2011c), concluding that the SZ signal correlates well with weak lensing mass. The intrinsic scatter that they measure is smaller but consistent with the results from Marrone et al. (2012).

The SZ signal can be predicted using X-ray observations. As discussed in §2.4, Kravtsov et al. (2006) introduced an X-ray analog of Y_{SZ} , Y_X , which is the product of the gas mass and the spectroscopic X-ray temperature. The comparison between Y_{SZ} and Y_X provides information on the ICM inner structure and especially the clumpiness. Indeed, as aforementioned, the quadratic and linear dependence of the X-ray and SZ signal on n_e for Y_X and Y_{SZ} respectively enable us to equate Y_X and Y_{SZ} only if the gas distribution is completely smooth, i.e. $\langle n_e^2 \rangle = \langle n_e \rangle^2$.

From these early studies, no consensus was reached whether predictions for the SZ signal based on ICM properties from X-ray observations are in agreement with direct SZ observations. Lieu et al. (2006) and Bielby & Shanks (2007) found evidence for a weaker SZ signal than expected from X-ray predictions in the WMAP3 data. This case was strengthened by the WMAP7 data analysis (Komatsu et al. 2011) which argues for a deficit of SZ signal, especially at low halo masses. However, re-analysing the same data, Afshordi et al. (2007) and Melin et al. (2011) found a good agreement between the SZ measurements and X-ray predictions. These conflicting results have demonstrated the need for more precise SZ measurements for larger samples of clusters from dedicated and multi-wavelength surveys in order to improve our understanding of cluster physics and cosmology.

4.2 SZ scaling relations: first results from large dedicated SZ surveys

Thanks to the start of wide-area SZ surveys, performed with dedicated instruments, there has been a lot of progress in recent years. Indeed, from the current generation of high sensitivity, high resolution and large coverage microwave telescopes (such as *Planck*, ACT, and SPT), new cluster surveys are producing catalogues of hundreds of SZ-detected clusters including new high-redshift objects. These numbers will continue to increase in the next few years.

The first clusters discovered in a blind SZ survey were reported by Staniszewski et al. (2009) who used data from the South Pole Telescope (SPT; Carlstrom et al. 2011) and demonstrated the capability of the SZ signal for cluster-finding. Hincks et al. (2010), Vanderlinde et al. (2010) and Marriage et al. (2011) reported more blind cluster detections (each ~ 20 candidates), setting the stage for SZ selected cluster catalogs.

SPT and ACT have been able to realize blind detections from ground based facilities because they combine three essential design features: resolution matched to the size of the cluster, degree-scale field of view for efficient surveying and the unprecedented sensitivity of bolometric detector arrays with 1000 elements. These observations have also demonstrated the need for multi-wavelength observations for a blind SZ survey in order to reduce the contamination from astrophysical foreground and background, as well as from primary CMB anisotropies. For instance the aforementioned SPT results were obtained with a single band survey (150 GHz) and the contamination hampered the determination of the aperture size required to integrate the SZ flux. Since the uncertainty on the scale aperture greatly affects the relation between Y_{SZ} and total mass, the SPT detection significance has been used as a mass proxy rather than Y_{SZ} in these initial studies.

The *Planck* satellite, launched in 2009, will soon provide the first multi-band, all-sky catalog of blind SZ detections. This catalog will be nearly mass selected and less affected by the systematics of X-ray selection. This makes the SZ signal a very attractive alternative for an unbiased proxy of the cluster mass (Vanderlinde et al. 2010; Williamson et al. 2011). The early release from the *Planck* Collaboration consists of 189 SZ extended sources at low/intermediate redshift (i.e., the ESZ sample; Planck Collaboration et al. 2011c). Although most of the clusters in this catalog were previously detected (either in the optical or in the X-ray band), the sample also contains 20 clusters discovered by *Planck*. Twelve of these have been confirmed with XMM-Newton (Planck Collaboration et al. 2011a), and 8 remained unconfirmed cluster candidates. Seven were further confirmed by targeted observations with SPT (Story et al. 2011), AMI (Planck Collaboration et al. 2013a), Bolocam (Sayers et al. 2012) and CARMA (Muchovej et al. 2012).

Recently the SPT collaboration released a new extended sample of 224 SZ clusters detected at 150 GHz in an area of 750 sq. deg., drastically increasing the number of SZ detected clusters (Reichardt et al. 2013). More than half (117) of the systems in this catalog are new detections. Part of the sample was used, together with other probes, to constrain cosmology (Benson et al. 2013). More recently the ACT collaboration published a sample of 68 clusters out of which 19 were new discoveries (Hasselfield et al. 2013).

Planck released some early results on scaling relations derived from three main studies, each using a different approach. The first is a statistical study of scaling relations by Planck Collaboration et al. (2011b) starting from a X-ray selected sample of about 1600 galaxy clusters drawn from the X-ray meta catalog (MCXC) by Piffaretti et al. (2011).

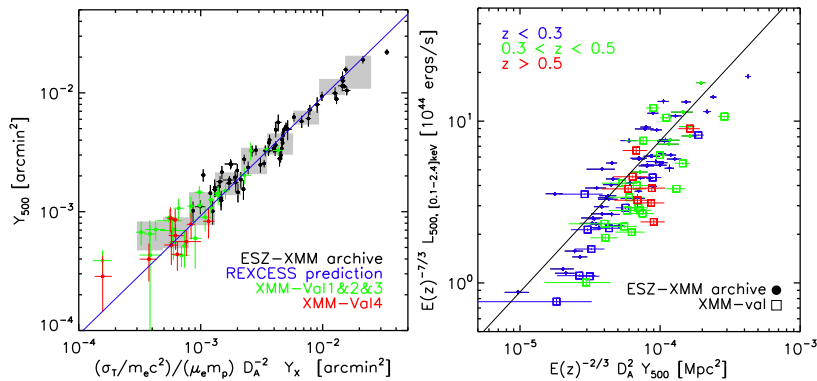


Fig. 7 Scaling properties from *Planck* studies. (*left*) Relation between Y_X and Y_{500} for the new detected clusters confirmed by XMM-Newton (red and green dots) and of the ESZ clusters with XMM-Newton archive data (black dots). The blue solid line shows the prediction from the REXCESS sample measurements. Credit:Planck Collaboration, A&A, Vol. 550, pg. 130, 2013, reproduced with permission © ESO. (*right*) Scaling relations between the X-ray luminosity and Y_{500} for new *Planck* clusters confirmed by XMM-Newton (squares) and for the ESZ clusters with XMM-Newton archive data (dots). Each quantity is scaled with redshift, as expected from standard self-similar evolution. The solid black lines denote the predicted Y_{500} scaling relations from the REXCESS X-ray observations (Arnaud et al. 2010). Credit:Planck Collaboration, A&A, Vol. 550, pg. 130, 2013, reproduced with permission © ESO.

This study combined the accuracy of the *Planck* measurements with the statistical size of the sample to overcome the dispersion within individual measurements and recovered X-ray–SZ scaling relations consistent with the predictions from X-ray constraints. The intrinsic scatter in the $D_A^2 Y_{500} - L_{X,500}$ relation amounts to $\sim 40\%$ and it is likely due to variation in the dynamical states of the clusters. Planck Collaboration et al. (2011d) studied a subsample of 62 local ($z \leq 0.4$) clusters from the ESZ sample for which high quality XMM-Newton archive data were available. This study confirmed the agreement between the SZ and X-ray scaling relations. A remarkably small logarithmic intrinsic scatter (10%) in the $D_A^2 Y_{500} - Y_{X,500}$ relation was derived, consistent with the idea that both quantities are low-scatter mass proxies.

Finally Planck Collaboration et al. (2011a), Planck Collaboration et al. (2012) and Planck Collaboration et al. (2013b) analysed a sample of 37 newly detected clusters by *Planck* that were confirmed with XMM-Newton as single systems. This study revealed a non-negligible population of massive dynamically perturbed objects with low X-ray surface brightness, lying around or below the flux limit of X-ray surveys such as REFLEX and NORAS (Böhringer et al. 2000, 2004). In this *Planck* sample the proportion of objects with a perturbed dynamical state tops $\sim 70\%$, which is to be compared to the $\sim 30\%$ observed in the X-ray selected representative REXCESS sample (Böhringer et al. 2007). These clusters have much flatter density profiles, lower X-ray luminosity and a more disturbed morphology when compared to X-ray selected samples. These SZ selected clusters show a larger scatter in the plane of the scaling relations involving Y_X or L_X with respect to the X-ray selected ones (see Fig. 7).

The consistency of these three approaches and results highlights the very good agreement between the SZ and X-ray measurements of the intra-cluster medium, at least within a radius of R_{500} . Similar results drawn from smaller samples of clusters spreading over a wider range of redshifts derived by SPT (Andersson et al. 2011) and

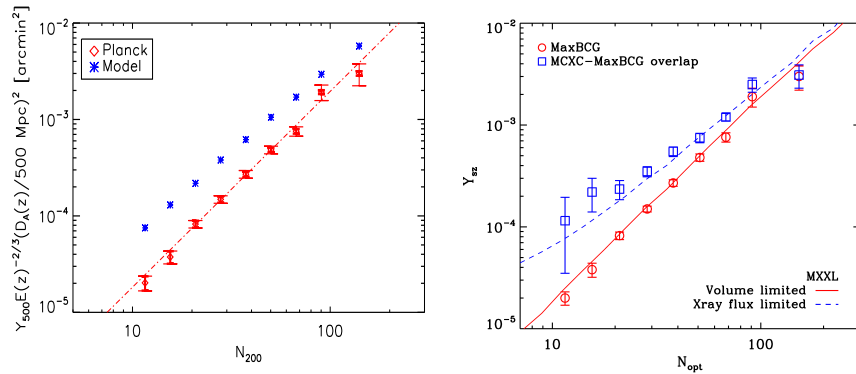


Fig. 8 The optical richness versus the SZ flux scaling relation. *Left*: Measured from stacking the signal at the location of the maxBCG clusters in the *Planck* survey (reprinted from Fig 2, right panel of Planck Collaboration et al. 2011e). Red diamonds and blue triangles mark the data and predicted signal from the X-ray constraints respectively. *Right*: Obtained from mock samples built from the XXL simulations for an optical maxBCG like catalogue (red squares) and the overlap between a maxBCG and MCXC like catalogues (blue squares) showing the differences obtained from the *Planck* measurements could be an effect of combined selection biases (reprinted from Fig 11, right panel of Angulo et al. 2012).

ACT (Marriage et al. 2011) also agree with the *Planck* findings. It is, however, important to test the effects of clumping or assumptions of hydrostatic equilibrium by comparing to observations that are not related to the ICM. Comparison to weak lensing masses were discussed above. Alternatively one can compare to dynamical masses, which was done in Rines et al. (2010) and Sifon et al. (2012).

Planck Collaboration et al. (2011e) used an optically selected sample (maxBCG; Koester et al. 2007) to investigate the stacked relation between SZ signal and weak lensing mass. The derived amplitude is found to be significantly lower than when X-ray masses are used. The two relations are shown in the left panel of Figure 8. To date a conclusive explanation of this discrepancy has not been presented, although it is expected to arise from the cumulative effect of various biases. For instance, a bias in the weak-lensing mass measurements and/or a high contamination of the optical catalogue have been proposed as possible explanations; a bias in the hydrostatic X-ray masses relative to the weak-lensing based ones can also cause a different normalization (e.g. Nagai et al. 2007; Mahdavi et al. 2008, 2012), although the required level of bias would be much larger than is expected from simulations and observations. Angulo et al. (2012) used simulated clusters from the new Millennium-XXL simulations to show that the discrepancy in the amplitude can result from the Malmquist bias in flux limited samples. In this case the discrepancy would arise from the propagation of the Malmquist bias from the X-ray luminosities to the SZ signal through covariance in their scatter at fixed cluster mass (Fig. 8, right panel). Clearly a better understanding of the link between the X-ray, lensing and SZ constraints on the cluster mass should help to achieve a better definition and understanding of the mass proxies for galaxy clusters.

5 Optical scaling relations

The total mass of a galaxy cluster can be directly estimated using spectroscopic measurements of the projected velocity dispersion of the member galaxies by applying the virial theorem under the assumption of dynamical equilibrium (Zwicky 1933). The mass enclosed within a radius, r , is given⁷ by the Jeans equation (e.g. Binney & Tremaine 1987):

$$M(r) = -\frac{r\sigma_r^2(r)}{G} \left[\frac{d \ln \rho}{d \ln r} + \frac{d \ln \sigma_r^2(r)}{d \ln r} + 2\beta(r) \right], \quad (26)$$

where $\rho(r)$ is the galaxy number density, σ_r the radial component of the velocity dispersion and $\beta(r) = 1 - \sigma_t^2(r)/\sigma_r^2(r)$ the isotropy parameter, which characterizes the ratio of the tangential to the radial dispersion.

If we consider for simplicity an isothermal system with an isotropic velocity field the second and third terms vanish. In this case it becomes clear that the velocity dispersion as a function of radius and the radial distribution of a galaxy population are not independent variables, but must be balanced to provide the correct mass of the system.

By applying the virial theorem (which is an integration of the Jeans equation; Binney & Tremaine 1987), we obtain that the total virial mass of the cluster (M_V) depends on the global velocity dispersion (σ) and the spatial distribution of the galaxy population. In the approximation that the galaxies trace the matter perfectly, we obtain

$$M_V = \frac{\sigma^2 R_V}{G} = \frac{3\pi\sigma_P^2 R_{V,P}}{2G}, \quad (27)$$

where R_V is the virial radius. In the spherical approximation $\sigma^2 = 3\sigma_P^2$ and it is possible to express the virial mass in terms of the projected radius and line-of-sight velocity dispersion (respectively $R_{V,P}$ and σ_P) as in the second part of Eqn. 27. This estimator has the advantage over the Jeans equation that it uses the integrated quantity σ_P rather than the dispersion profile. For this reason Eqn. 27 is the most commonly used to estimate the virial mass (Girardi et al. 1998).

Compared to X-ray observations, an advantage of using galaxies as tracers is that the galaxy population can be observed with good accuracy out to large radii. In the cluster outskirts, where the virial equilibrium assumption does not hold, the caustic method has yielded promising results for the total cluster masses (e.g., Rines et al. 2003; Diaferio et al. 2005; Rines et al. 2013). The accuracy of dynamical methods was studied in detail by Biviano et al. (2006), who found that the virial estimator can recover the virial mass for a galaxy cluster within 10% for samples of at least 60 cluster members. In this sense, the dynamical approach is expensive in terms of telescope time.

For this reason, especially considering large cluster samples, it is interesting to consider inexpensive proxies based on the global optical properties of clusters. Given that the gas fraction f_{gas} appears to be a low-scatter mass proxy (see §2.4), one might expect observations of the stellar content to yield good proxies. This reasoning suggests that the total optical luminosity (L_{op}) or richness (N_{gal}) of a galaxy cluster provides a direct indication of its mass. Such optical mass proxies are relatively inexpensive to measure, requiring only direct images of moderate depth, even for high redshift clusters.

⁷ As was the case for X-ray observations: T_X is now replaced by the velocity dispersion σ which can be interpreted as the “temperature” of the galaxy distribution.

Furthermore, these estimators are applicable to low mass groups that typically lack a sufficient number of member galaxies for a robust dynamical mass estimation.

N_{gal} and L_{op} are simply evaluated by counting galaxies or summing their luminosities in an aperture down to a certain magnitude. If the sample is incomplete, a correction must be applied. Both N_{gal} and L_{op} must be corrected for the expected contamination by field galaxies. The latter can be estimated from a comparison with the surrounding field where no cluster was detected or from the number counts of blank-field galaxy surveys.

The relation between optical and X-ray observables was studied by Yee & Ellingson (2003) and Popesso et al. (2004). The latter combined observations of 114 clusters of galaxies in the SDSS and RASS. They found that the luminosity in the red optical bands (i and z), which are more sensitive to the light of the old stellar population and therefore to the stellar mass of cluster galaxies, have tight correlations with the X-ray properties. Furthermore Popesso et al. (2004) found that by using L_{op} (in the z -band) it is possible to predict the temperature of the cluster (and thus the mass) with an precision of 60%. More recently Lopes et al. (2009) found that the scatter between optical luminosity and X-ray temperature for a sample of massive clusters amounts to 40%, which is comparable to that of the corresponding relation based on X-ray data alone.

Lack of multi-colour data results in potentially large corrections for the background, thus increasing the uncertainties in the richness estimates. Nowadays, optical cluster surveys employ multiple bands, which improves the purity of the samples and provides photometric redshift estimates, thanks to the well-known observation that early-type galaxies form a tight ridgeline in color–magnitude space. With the advent of large optical surveys aimed at constraining cosmology, more effort is being spent on refining these mass proxies.

Current large optically selected cluster samples, such as the maxBCG sample (Koester et al. 2007), have been used to study the relation between total mass and optical observables. Mass estimates of the clusters in the maxBCG sample were derived via a stacked weak lensing analysis (Johnston et al. 2007) by binning the clusters in richness. For this sample Rykoff et al. (2008b) studied the relation between the X-ray luminosity and weak lensing mass. The measurements indicate a power-law relation between mass and richness. Rozo et al. (2009a) measured a logarithmic scatter in mass at fixed richness of $\sigma_{\ln M|N_{200}} = 0.45^{+0.20}_{-0.18}$ (with 95% confidence) at $N_{200} \approx 40$, where N_{200} is the number of red-sequence galaxies within r_{200} . Sheldon et al. (2009) measured the optical luminosities of the clusters in this sample. They found that the signal within a given richness bin depends on luminosity, which suggests that the luminosity is more closely correlated with mass than N_{gal} . These studies have drawn attention to optical scaling relations as a very effective way to obtain mass estimates for a large number of systems.

Optical scaling relations are generally more difficult to interpret because their behaviour cannot be predicted from simple physics scaling arguments (with the possible exception of the stellar mass). This is because the observed galaxy properties are the end result of the complicated non-linear process of galaxy formation and evolution. The $M_{\text{tot}} - L_{\text{op}}$ relations have power law slopes close to unity, but not quite so, as most studies indicate an increase of the mass-to-light ratio M/L_{op} with cluster mass. This is a direct consequence of the variation of the fraction of stars in galaxies (Lin et al. 2003; Giodini et al. 2009), suggesting that the efficiency of star formation or galaxy

evolution processes depend on the total mass. We note that these same processes may also affect the ICM properties in low mass systems.

The mass-richness relation shows a large intrinsic scatter (Gladders et al. 2007; Rozo et al. 2009a), which is mostly caused by the large Poisson noise due to the low number of galaxies. It is possible to reduce the scatter using more optimal estimators. For example (Roza et al. 2009b, 2011) improved on the estimation of the richness parameter, obtaining a significant reduction of the scatter in mass at fixed richness for maxBCG clusters, by using a matched filter and an optimized iterative measure of the cluster extent (also see Rykoff et al. 2012). Andreon & Hurn (2010) investigated the mass-richness relation using caustic mass measurements for a sample of local X-ray detected clusters. They stressed that once a careful statistical analysis is performed, the richness has a similar performance as the X-ray luminosity in predicting the total mass of a cluster.

6 Interpretation of scaling relations with simulations

Only under certain (ideal) conditions we can derive scaling relations between the baryonic properties and the total mass. However, observations indicate the real situation is more complicated and we need to rely on numerical simulations to gain further insights. The simulation box represents a controlled laboratory where the models can be tested and compared directly with the constraints derived from observations. Simulations start from a set of initial conditions which consist of a realization of a density field with statistical properties (e.g. the power spectrum) appropriate for the adopted background cosmological model. The evolution of these initially small density fluctuations is followed by advancing the density and velocity fields forward by numerically integrating the equations governing the dynamics of dark matter and baryons. The evolution of the collision-less dark matter is relatively easily implemented, but including the effects of baryons has proven to be more complicated. For a recent review on cosmological simulations of galaxy clusters we refer the interested reader to Borgani & Kravtsov (2011).

The best way to test if simulations correctly model the various physical processes is to examine whether they faithfully reproduce the statistical properties of a cluster sample, such as the observed scaling relations. While a simple gravity-only simulation naturally reproduces the scaling relations for massive galaxy clusters (as they are mostly self-similar), more physics needs to be included to reproduce the observed deviations from the purely gravitational scenario.

Radiative cooling was one of the first processes to be explored in simulations. As discussed by Bryan (2000), it can cause a selective removal of the low entropy gas from the hot phase. Simulations show that including radiative cooling leads to somewhat steeper scalings of the X-ray luminosity relations by reducing the fraction of hot gas in a mass dependent fashion. However, the effect is not sufficient to reproduce the observed steepening (Davé et al. 2002). Furthermore, a “cooling only scenario” suffers from an excessive conversion of gas into stars in the densest cluster regions (“overcooling”; Blanchard et al. 1992, Balogh et al. 2001), leading to an unreasonably high predicted baryon fraction in the cores of galaxy clusters (Kravtsov et al. 2005). Given the short gas cooling time this should lead to significant star formation, which is not observed; nor is the cold gas (e.g. Kaastra et al. 2001; Peterson et al. 2003).

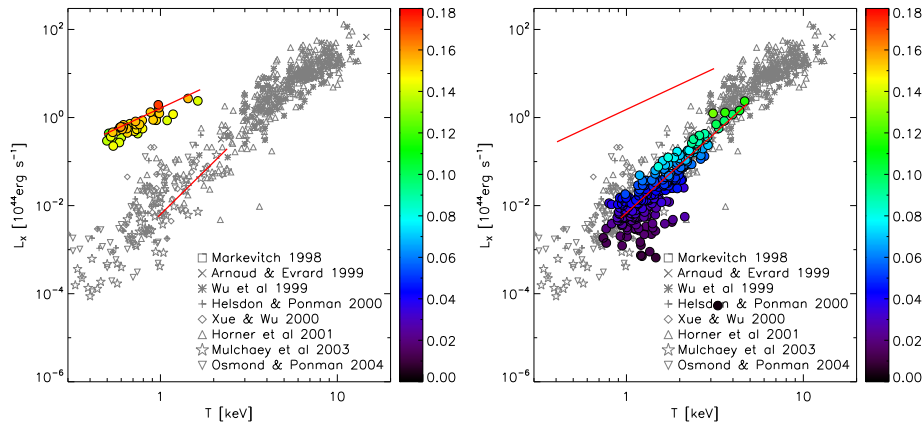


Fig. 9 Effect of feedback on simulated scaling relations (colored circles) between X-ray luminosity and temperature from Short & Thomas (2009) plotted on top of observed data-points (in gray). On the left the simulation include only supernova feedback, while on the right AGN feedback is included, where the energy is strongly coupled with the gas. It is clear that an energetic event similar to the latter is needed to reproduce the observed scaling. (Reproduced by permission of the AAS)

A solution can be provided by a suitable scheme of gas heating that compensates for the radiative losses, pressurizes the gas in the core regions, and regulates star formation. Feedback from supernovae is in principle a good candidate to regulate gas cooling in cluster cores. The energy injected by the supernova explosions can be used to keep the relatively low-entropy gas in the hot phase despite its short cooling time. Although this is a plausible mechanism, stellar feedback is generally not considered the complete solution because the heating is thought to be insufficient to reproduce the observed $L_X - T$ relation (see Fig. 9). Another observation is that the brightest cluster galaxies contain mostly old stellar populations that are not capable of providing the needed amount of energy to offset the cooling (although star formation is observed in cool core clusters (e.g. Crawford et al. 1999; Edge 2001; Edwards et al. 2007; Bildfell et al. 2008)).

Therefore another (powerful) feedback process is needed. Furthermore, it should not be related directly to star formation activity. The most popular candidate that appears to fit the bill is AGN feedback. The energy output of the AGN is provided by the accretion energy released by the gas surrounding the supermassive black hole at the center of the central cluster galaxy. There is convincing observational evidence suggesting that AGN feedback has a large impact on the surrounding gas. At radio wavelengths observations show large bubbles of relativistic gas being spewed from the central galaxies and their locations overlap with large cavities in the X-ray luminous gas (e.g. Fabian et al. 2006). The amount of energy that is injected is sufficiently large to offset the cooling and affect the cluster gas in the core and beyond. Furthermore its effect will be even more dramatic in low mass groups, where the injected energy can be comparable to the binding energy of the gas (e.g. Giodini et al. 2010). AGN heating is nowadays considered the most likely mechanism, also because it is thought to play an important role in quenching the star formation in the brightest cluster galaxy,

which otherwise ends up too luminous in the simulations. Finally, trends of the hot gas fraction and entropy with cluster mass also support AGN heating.

The main challenge for simulators is that the details of the heating mechanism are still poorly understood. First of all it is unknown how the coupling between the AGN energy injection and the ICM occurs. Furthermore, AGN heating works through episodic jets, but it is not clear how the cooling and the heating episodes may be tuned. In the past years the first attempts to include AGN heating in full cosmological simulations have been carried out. Sijacki & Springel (2006) developed a model for AGN heating via hot thermal bubbles in a cosmological simulation of cluster formation. Puchwein et al. (2008) have shown that the observed $L_X - T$ relation is successfully reproduced without invoking excessive cooling in the central region of the simulated clusters. However this model does fail to reproduce the observed entropy profiles. McCarthy et al. (2010) used simulated groups from the Overwhelmingly Large Simulations project (Schaye et al. 2010). In these simulations AGN feedback is included to match the observed relation between black hole mass and the galaxy bulge mass (Booth & Schaye 2010). Encouragingly, they find entropy profiles and an $L_X - T$ relation similar to the observations. Short & Thomas (2009) reproduce the observed scaling relations with simulations where feedback from galaxies is incorporated via a hybrid approach: the energy imparted to the ICM by SNe and AGN is computed from a semi-analytic model of galaxy formation.

The observed deviation from self-similarity can also be explained by pre-heating of the gas at early times. This is mostly motivated by observational results that indicate the existence of an universal entropy floor for clusters (Evrard & Henry 1991; Kaiser 1991). In this scenario, the energy injection into the ICM from nongravitational processes such as supernovae, star formation, and galactic winds heats the gas at high redshift, before the gas collapses in the deep cluster/group potential well, causing a high-redshift entropy modification. Simulations show that the increase in entropy arises from the shift from clumpy to smooth accretion in the cluster outskirts due to the heating (Borgani et al. 2005). The extra entropy would inhibit the gas from falling into the potential well. The effect would be larger for low mass systems which have shallower potentials, alleviating the discrepancy between simulations and observations. However, simulations have shown that the resulting entropy profiles of the simulated groups are much too flat compared to observations (Borgani et al. 2005; Younger & Bryan 2007). Therefore the observed lack of iso-entropic core entropy profiles in groups and poor clusters has shown that simple preheating is unlikely to be the sole explanation of the observations (Ponman et al. 2003; Pratt & Arnaud 2003).

Ettori et al. (2004b) using a simulation that included radiative cooling, star formation and supernova feedback, found a significant negative evolution in the normalization of the $L_X - T$ and $S - T$ relations in objects selected in the range $0.5 < z < 1$. This result suggests either that the hot X-ray-emitting plasma measured in the central regions of simulated systems is smaller than the observed one or that systematically higher values of gas temperatures are recovered in the simulated dataset. Muanwong et al. (2006) and Kay et al. (2007) using different prescriptions for cooling and stellar feedback found qualitatively similar results.

Muanwong et al. (2006) used three hydrodynamic simulations in the Λ CDM cosmology. They considered a “radiative-cooling”, “pre-heating” and “AGN-feedback” scenario. They concluded that all the models could reproduce the observed local $L_X - T$ scaling relation but substantial differences between the models are predicted at $z = 1.5$.

According to these simulations, if the evolution of the scaling relation is parametrized as

$$L_{\text{bol}} = C_0 \times T_{\text{bol}}^\alpha \times (1+z)^A, \quad (28)$$

the value of A at $z = 1.5$ is predicted to be ~ -0.6 (mildly negative evolution) for the AGN feedback model, ~ 0.7 (mildly positive evolution) in a pre-heating scenario and ~ 1.9 (strong positive evolution) for a radiative cooling model.

Current observational constraints (see §3) would support a mildly positive evolution, pointing towards early and widespread preheating of the ICM, to be preferred over an extended period of preheating. Short et al. (2010), using the Millennium Gas Simulations which include AGN feedback following Short & Thomas (2009), confirms the different model predictions but concludes that the feedback model is favoured for $z \leq 0.5$ while the preheating model is preferred at higher redshift, when comparing simulations to recent observations by Pratt et al. (2009) and Maughan et al. (2008). There remain, however, concerns about strong selection biases in the current samples of high-redshift clusters.

7 Some general considerations

Any survey of galaxy clusters provides catalogs of systems that are somewhat biased and incomplete. Biases and incompleteness arise because of the chosen survey strategy or simply due to the finite sensitivity. Furthermore the distribution of cluster properties is not uniform in the observable-mass plane, but there is segregation (e.g. cool-cores segregate at high luminosity). Therefore the determination of correct scaling relations relies heavily on understanding the statistical properties of the underlying population and any bias in the observables. In this section we list some of the issues that need to be considered when determining and interpreting mass-observable scaling relations.

- *Malmquist bias*: the empirical determination of scaling relations is complicated by selection effects in the observations due to the presence of scatter. For instance, in an X-ray flux limited survey the intrinsically brighter sources for a given mass will appear to be more numerous than the fainter sources at that same mass because they can be seen in a larger volume (brighter sources are seen out to larger distances). This bias is commonly known as Malmquist bias and should be taken into account in both the scaling relation calibration and the cosmological analysis based on such relations. Some works in which this bias has been properly taken into account in the interpretation of scaling relations are Ikebe et al. (2002), Stanek et al. (2006), Pacaud et al. (2007), Pratt et al. (2009), Vikhlinin et al. (2009a). Mittal et al. (2011) even applied individual Malmquist bias corrections for SCC, WCC, and NCC clusters.
- *Eddington bias*: this is the bias caused by the uncertainty in the observables in the sample (Eddington 1913). In general, sources of a given X-ray luminosity, for instance, will follow a distribution associated with the uncertainty in the measurement. Because the X-ray luminosity function is non-uniform (there are more objects with low luminosity) a larger fraction of systems will scatter from low luminosity to high than vice-versa, flattening the distribution. Another complication arises if there is a detection threshold, e.g. a flux limit. In this case the full range in scatter is not well represented at low luminosities and the inferred average luminosity will

-
- be overestimated. For examples in the context of X-ray scaling relations see for example Allen et al. (2011) or Maughan et al. (2012).
- *Hidden priors*: the scatter of the points around an mass-observable scaling relation depends on the underlying cosmology, because it is directly linked to the shape of the halo mass function (Staneke et al. 2006). Some authors (e.g. Mantz et al. 2010a; Allen et al. 2011) have recently started performing joint fits of scaling relations and cosmological parameters.
 - *Binning of noisy data*: scaling relations are often estimated from binned data, instead of individual clusters. However particular care must be taken when the observable chosen for the binning is very noisy. With a large scatter, the mean values used to compute the ensemble averaged values may be biased with respect to the median relation, which is more robust. This is because the scatter about the mean is typically described by a lognormal distribution, and as a result the mean values will be dominated by the most luminous clusters. Considering the $L_X - N_{\text{gal}}$ relation as an example, the stacked normalization overestimates the median by a factor $\exp(\sigma_{\ln L_X}/2)$, as discussed in Rykoff et al. (2008a). As the scatter may depend on the mass, this can also impact the recovered slope. Hence, the intrinsic scatter as a function of the various cluster properties needs to be known to account for this. Also covariance between observables needs to be accounted for. Note that this is also true for unbinned noisy data, although such analyses are often restricted to higher masses.
 - *Cluster type bias*: flux-limited samples preferentially select certain types of clusters. For instance, Hudson et al. (2010) and Mittal et al. (2011) showed that due to the enhanced L_X for a given T_X (or M), clusters with cool cores are overrepresented in an X-ray survey. Similarly, Eckert et al. (2011) showed that the detection efficiency of X-ray instruments is not the same for centrally peaked (CC) and flat (NCC) objects; they quantified this dependence on the surface brightness and corrected the corresponding fractions. Note that both effects should be accounted for, which has not been done simultaneously in any study up to now.
 - *Archive bias*: corrections for Malmquist, Eddington, and cluster type bias can only be applied to samples that are complete according to (relatively) simple selection criteria, e.g., X-ray flux-limited samples. Samples constructed from public archives are, in general, not complete in any sense; their selection functions are often unknown and, therefore, such samples cannot be reproduced by mock simulations. Also, certain types of clusters may be preferred for proposals by observers and time allocation committees, e.g., strong cool core clusters or major mergers as opposed to more “boring” weak cool core clusters. Therefore, any scaling relation study aiming for high accuracy should be based on a complete sample, with appropriate corrections applied.
 - *Halo shape*: the assumption of spherical symmetry of the ICM, whereas clusters are known to be triaxial structures, can affect the observed scaling relations at the level of $\sim 10\%$ (e.g. Buote & Humphrey 2012) and introduces scatter. Hence knowledge of the intrinsic shape and orientation of halos is crucial for an unbiased determination of their masses. As reviewed in Limousin et al. (2012) multi-wavelength observations of the ICM and mass can be used to quantify and account for triaxiality.

8 Conclusions and Future Outlook

The next generation of X-ray observatories will provide powerful tools to probe the structure and mass-energy content of the Universe. Such probes will be complementary to the other planned cosmological experiments, such as *Planck*, *Euclid*⁸ (Laureijs et al. 2011) and LSST. They have the potential of placing very tight constraints on different classes of dark-energy models, possibly finding signatures of departures from the standard Λ CDM predictions. eROSITA (Predehl et al. 2010; Pillepich et al. 2012; Merloni et al. 2012) will produce cluster catalogs with $\sim 10^5$ objects out to redshift ~ 1 , increasing the current statistical samples by 1-2 orders of magnitude and extending the redshift range over which the growth of cosmic structures can be traced.

A number of infrared and optical surveys will provide the required complementary photometric and spectroscopic redshifts, some of which have already started collecting data. The photometric data will allow for the identification of the cluster members and will be used in combination with X-ray data to classify the eROSITA clusters. Furthermore, these data provide galaxy targets for additional spectroscopy if needed, and will also provide important shear information for background galaxies, enabling the calibration of the galaxy cluster masses through weak lensing analyses (see Hoekstra et al. 2013, for a review). Importantly, these surveys can themselves be used to search for clusters, resulting in large multi-wavelength databases of clusters.

A few thousand clusters will also have their temperatures determined directly from the eROSITA survey data. This will help to reduce the scatter in the mass measurements for individual clusters providing tighter constraints on the scaling relations. Thanks to these numbers, eROSITA will permit to tackle several crucial astrophysical issues, such as:

- the cluster mass function and its evolution, $N(M, z)$, that provide constraints on the matter density, the amplitude of the primordial power spectrum and dark energy (e.g. Vikhlinin et al. 2009b);
- the angular clustering as a function of redshift (e.g. Valageas & Clerc 2012);
- the cluster baryon fraction as function of the redshift, which constrains the dark matter and energy densities (e.g. Allen et al. 2008; Ettori et al. 2009);
- the baryonic wiggles due to acoustic oscillations at recombination, which will give tight constraints on the space curvature and cosmological parameters (e.g. Amendola et al. 2012);
- the spatially-resolved baryonic and total mass distribution over the entire virial region for a subset of the X-ray bright systems with complementary SZ and lensing data.

To reduce both the statistical and systematic uncertainties in these measurements further, an X-ray telescope with the specifications of the concepts such as *Athena* (e.g. Barcons et al. 2012) or *Wide Field X-ray Telescope* (e.g. Rosati et al. 2010) is required. For instance, to improve the characterization of the thermodynamical properties of X-ray emitting galaxy clusters as well as the mass modeling, spatially-resolved temperatures of the ICM out to $z \sim 1$ and beyond are required. To evaluate the thermal structure of the ICM and how the scaling relations among integrated quantities depend on the energy feedback from, e.g., mergers, AGNs and supernovae, high

⁸ <http://www.euclid-ec.org>

resolution spectroscopy, hard X-ray imaging and follow-up observations in radio, optical and infrared bands are needed. In the near future, NuSTAR (launched in 2012; <http://www.nustar.caltech.edu/>), ASTRO-H (to be launched in 2015; <http://astro-h.isas.jaxa.jp/>), LOFAR (e.g. van Weeren et al. 2012) and the optical/IR telescopes mentioned above will provide invaluable resources to deepen our knowledge on the ICM physical properties. Hence, despite the tremendous progress we reviewed here, much more is yet to be studied.

Acknowledgements We would like to thank ISSI for their hospitality. SG & HH acknowledge support from NWO Vidi grant 639.042.814. LL acknowledges support by the German Research Association (DFG) through grant RE 1462/6 and by the German Aerospace Agency (DLR) with funds from the Ministry of Economy and Technology (BMW) through grant 50 OR 1102. EP acknowledges the support from grant ANR- 11-BD56-015. SE acknowledges the financial contribution from contracts ASI-INAF I/023/05/0 and I/088/06/0. THR acknowledges support by the DFG through Heisenberg grant RE 1462/5 and grant RE 1462/6.

References

- Afshordi, N., Lin, Y.-T., Nagai, D., & Sanderson, A. J. R. 2007, *MNRAS*, 378, 293
- Aghanim, N., da Silva, A. C., & Nunes, N. J. 2009, *A&A*, 496, 637
- Aghanim, N., Hansen, S. H., & Lagache, G. 2005, *A&A*, 439, 901
- Akritas, M. G., & Bershad, M. A. 1996, *Astrophysical Journal*, 470, 706
- Albrecht, A., et al. 2006, *ArXiv Astrophysics e-prints*
- Allen, S. W., Evrard, A. E., & Mantz, A. B. 2011, *ARA&A*, 49, 409
- Allen, S. W., Rapetti, D. A., Schmidt, R. W., Ebeling, H., Morris, R. G., & Fabian, A. C. 2008, *MNRAS*, 383, 879
- Allen, S. W., Schmidt, R. W., & Fabian, A. C. 2001, *MNRAS*, 328, L37
- Amendola, L., Appleby, S., Bacon, D., Baker, T., Baldi, M., & et al. 2012, *ArXiv e-prints*
- Andersson, K., et al. 2011, *Astrophysical Journal*, 738, 48
- Andreon, S., & Hurn, M. A. 2010, *MNRAS*, 404, 1922
- Andreon, S., Trinchieri, G., & Pizzolato, F. 2011, *MNRAS*, 412, 2391
- Angulo, R. E., Springel, V., White, S. D. M., Jenkins, A., Baugh, C. M., & Frenk, C. S. 2012, *MNRAS*, 426, 2046
- Arnaud, M., & Evrard, A. E. 1999, *MNRAS*, 305, 631
- Arnaud, M., Pointecouteau, E., & Pratt, G. W. 2005, *A&A*, 441, 893
- . 2007, *A&A*, 474, L37
- Arnaud, M., Pratt, G. W., Piffaretti, R., Böhringer, H., Croston, J. H., & Pointecouteau, E. 2010, *A&A*, 517, A92
- Atrio-Barandela, F., Mückel, J. P., & Génova-Santos, R. 2008, *Astrophysical Journal, Letters*, 674, L61
- Balogh, M. L., Babul, A., & Patton, D. R. 1999, *MNRAS*, 307, 463
- Balogh, M. L., Pearce, F. R., Bower, R. G., & Kay, S. T. 2001, *MNRAS*, 326, 1228
- Barcons, X., Barret, D., Decourchelle, A., den Herder, J.-W., Dotani, T., & et al. 2012, *ArXiv e-prints*
- Basu, K., Zhang, Y.-Y., Sommer, M. W., Bender, A. N., Bertoldi, F., & et al. 2010, *A&A*, 519, 519
- Benson, B. A., Church, S. E., Ade, P. A. R., Bock, J. J., Ganga, K. M., Henson, C. N., & Thompson, K. L. 2004, *Astrophysical Journal*, 617, 829
- Benson, B. A., et al. 2013, *Astrophysical Journal*, 763, 147
- Bielby, R. M., & Shanks, T. 2007, *MNRAS*, 382, 1196
- Bildfell, C., Hoekstra, H., Babul, A., & Mahdavi, A. 2008, *MNRAS*, 389, 1637
- Binney, J., & Tremaine, S. 1987
- Birkinshaw, M. 1999, *Phys. Rep.*, 310, 97
- Birkinshaw, M., Gull, S. F., & Northover, K. J. E. 1978, *MNRAS*, 185, 245
- Birkinshaw, M., Hughes, J. P., & Arnaud, K. A. 1991, *Astrophysical Journal*, 379, 466
- Biviano, A., Murante, G., Borgani, S., Diaferio, A., Dolag, K., & Girardi, M. 2006, *A&A*, 456, 23

- Blanchard, A., Valls-Gabaud, D., & Mamon, G. A. 1992, *A&A*, 264, 365
- Böhringer, H., Dolag, K., & Chon, G. 2012, *A&A*, 539, A120
- Böhringer, H., Schuecker, P., Pratt, G. W., Arnaud, M., Ponman, T. J., & et al. 2007, *A&A*, 469, 363
- Böhringer, H., et al. 2000, *Astrophysical Journal*, Supplement, 129, 435
- . 2004, *A&A*, 425, 367
- Bonamente, M., Joy, M., LaRoque, S. J., Carlstrom, J. E., Nagai, D., & Marrone, D. P. 2008, *Astrophysical Journal*, 675, 106
- Booth, C. M., & Schaye, J. 2010, *MNRAS*, 405, L1
- Borgani, S., Finoguenov, A., Kay, S. T., Ponman, T. J., Springel, V., Tozzi, P., & Voit, G. M. 2005, *MNRAS*, 361, 233
- Borgani, S., Governato, F., Wadsley, J., Menci, N., Tozzi, P., & et al. 2001, *Astrophysical Journal*, Letters, 559, L71
- Borgani, S., & Kravtsov, A. 2011, *Advanced Science Letters*, 4, 204
- Bower, R. G. 1997, *MNRAS*, 288, 355
- Branchesi, M., Gioia, I. M., Fanti, C., & Fanti, R. 2007, *A&A*, 472, 739
- Bryan, G. L. 2000, *Astrophysical Journal*, Letters, 544, L1
- Bryan, G. L., & Norman, M. L. 1998, *Astrophysical Journal*, 495, 80
- Buote, D. A., & Humphrey, P. J. 2012, *MNRAS*, 421, 1399
- Carlstrom, J. E., Holder, G. P., & Reese, E. D. 2002, *ARA&A*, 40, 643
- Carlstrom, J. E., Joy, M., & Grego, L. 1996, *Astrophysical Journal*, Letters, 456,
- Carlstrom, J. E., et al. 2011, *PASP*, 123, 568
- Challinor, A., & Lasenby, A. 1999, *Astrophysical Journal*, 510, 930
- Chen, Y., Reiprich, T. H., Böhringer, H., Ikebe, Y., & Zhang, Y.-Y. 2007, *A&A*, 466, 805
- Cooray, A. R. 1999, *MNRAS*, 307, 841
- Crawford, C. S., Allen, S. W., Ebeling, H., Edge, A. C., & Fabian, A. C. 1999, *MNRAS*, 306, 857
- Cunha, C. E., & Evrard, A. E. 2010, *Physical Review D*, 81, 083509
- da Silva, A. J. C. 2004, *Astrophysics and Space Science*, 290, 167
- Dai, X., Bregman, J. N., Kochanek, C. S., & Rasia, E. 2010, *Astrophysical Journal*, 719, 119
- Davé, R., Katz, N., & Weinberg, D. H. 2002, *Astrophysical Journal*, 579, 23
- David, L. P., Slyz, A., Jones, C., Forman, W., Vrtilik, S. D., & Arnaud, K. A. 1993, *Astrophysical Journal*, 412, 479
- Désert, F.-X., et al. 1998, *New Astronomy*, 3, 655
- Diaferio, A., Geller, M. J., & Rines, K. J. 2005, *Astrophysical Journal*, Letters, 628, L97
- Eckert, D., Molendi, S., & Paltani, S. 2011, *A&A*, 526, A79
- Eckmiller, H. J., Hudson, D. S., & Reiprich, T. H. 2011, *A&A*, 535, A105
- Eddington, A. S. 1913, *MNRAS*, 73, 359
- Edge, A. C. 2001, *MNRAS*, 328, 762
- Edge, A. C., & Stewart, G. C. 1991, *MNRAS*, 252, 414
- Edwards, L. O. V., Hudson, M. J., Balogh, M. L., & Smith, R. J. 2007, *MNRAS*, 379, 100
- Ettori, S., De Grandi, S., & Molendi, S. 2002, *A&A*, 391, 841
- Ettori, S., Morandi, A., Tozzi, P., Balestra, I., Borgani, S., & et al. 2009, *A&A*, 501, 61
- Ettori, S., Rasia, E., Fabjan, D., Borgani, S., & Dolag, K. 2012, *MNRAS*, 420, 2058
- Ettori, S., Tozzi, P., Borgani, S., & Rosati, P. 2004a, *A&A*, 417, 13
- Ettori, S., et al. 2004b, *MNRAS*, 354, 111
- Evrard, A. E. 1990, *Astrophysical Journal*, 363, 349
- Evrard, A. E., & Henry, J. P. 1991, *Astrophysical Journal*, 383, 95
- Evrard, A. E., Metzler, C. A., & Navarro, J. F. 1996, *Astrophysical Journal*, 469, 494
- Fabian, A. C., Sanders, J. S., Taylor, G. B., Allen, S. W., Crawford, C. S., Johnstone, R. M., & Iwasawa, K. 2006, *MNRAS*, 366, 417
- Fassbender, R., et al. 2011, *New Journal of Physics*, 13, 125014
- Finoguenov, A., Guzzo, L., Hasinger, G., Scoville, N. Z., Aussel, H., & et al. 2007, *Astrophysical Journal*, Supplement, 172, 182
- Finoguenov, A., Jones, C., Böhringer, H., & Ponman, T. J. 2002, *Astrophysical Journal*, 578, 74
- Finoguenov, A., Reiprich, T. H., & Böhringer, H. 2001, *A&A*, 368, 749
- Fox, D. C., & Loeb, A. 1997, *Astrophysical Journal*, 491, 459
- Gastaldello, F., Buote, D. A., Humphrey, P. J., Zappacosta, L., Bullock, J. S., Brighenti, F., & Mathews, W. G. 2007, *Astrophysical Journal*, 669, 158

- Giodini, S., Pierini, D., Finoguenov, A., Pratt, G. W., Boehringer, H., & et al. 2009, *Astrophysical Journal*, 703, 982
- Giodini, S., et al. 2010, *Astrophysical Journal*, 714, 218
- Girardi, M., Giuricin, G., Mardirossian, F., Mezzetti, M., & Boschin, W. 1998, *Astrophysical Journal*, 505, 74
- Gladders, M. D., Yee, H. K. C., Majumdar, S., Barrientos, L. F., Hoekstra, H., Hall, P. B., & Infante, L. 2007, *Astrophysical Journal*, 655, 128
- Hand, N., Addison, G. E., Aubourg, E., Battaglia, N., Battistelli, E. S., & et al. 2012, *ArXiv e-prints*
- Hasselfield, M., et al. 2013, *ArXiv e-prints*
- Henry, J. P., Evrard, A. E., Hoekstra, H., Babul, A., & Mahdavi, A. 2009, *Astrophysical Journal*, 691, 1307
- Herbig, T., Lawrence, C. R., Readhead, A. C. S., & Gulkis, S. 1995, *Astrophysical Journal, Letters*, 449,
- Hincks, A. D., et al. 2010, *Astrophysical Journal, Supplement*, 191, 423
- Hoekstra, H., Bartelmann, M., Dahle, H., Israel, H., Limousin, M., & Meneghetti, M. 2013, *ArXiv e-prints*
- Hoekstra, H., Mahdavi, A., Babul, A., & Bildfell, C. 2012, *MNRAS*, 427, 1298
- Hogg, D. W., Bovy, J., & Lang, D. 2010, *ArXiv e-prints*
- Holzappel, W. L., Wilbanks, T. M., Ade, P. A. R., Church, S. E., Fischer, M. L., Mauskopf, P. D., Osgood, D. E., & Lange, A. E. 1997, *Astrophysical Journal*, 479,
- Huang, C.-W. L., Wu, J.-H. P., Ho, P. T. P., Koch, P. M., & Liao, e. a. 2010, *Astrophysical Journal*, 716, 758
- Hudson, D. S., Mittal, R., Reiprich, T. H., Nulsen, P. E. J., Andernach, H., & Sarazin, C. L. 2010, *A&A*, 513, A37
- Ikebe, Y., Reiprich, T. H., Böhringer, H., Tanaka, Y., & Kitayama, T. 2002, *A&A*, 383, 773
- Johnston, D. E., et al. 2007, *ArXiv e-prints*
- Juett, A. M., Davis, D. S., & Mushotzky, R. 2010, *Astrophysical Journal, Letters*, 709, L103
- Kaastra, J. S., Ferrigno, C., Tamura, T., Paerels, F. B. S., Peterson, J. R., & Mittaz, J. P. D. 2001, *A&A*, 365, L99
- Kaiser, N. 1986, *MNRAS*, 222, 323
- . 1991, *Astrophysical Journal*, 383, 104
- Kashlinsky, A., Atrio-Barandela, F., Ebeling, H., Edge, A., & Kocevski, D. 2010, *Astrophysical Journal, Letters*, 712, L81
- Kay, S. T., da Silva, A. C., Aghanim, N., Blanchard, A., Liddle, A. R., Puget, J.-L., Sadat, R., & Thomas, P. A. 2007, *MNRAS*, 377, 317
- Kitayama, T., Komatsu, E., Ota, N., Kuwabara, T., Suto, Y., Yoshikawa, K., Hattori, M., & Matsuo, H. 2004, *Publications of the ASJ*, 56, 17
- Koester, B. P., et al. 2007, *Astrophysical Journal*, 660, 239
- Komatsu, E., Kitayama, T., Suto, Y., Hattori, M., Kawabe, R., Matsuo, H., Schindler, S., & Yoshikawa, K. 1999, *Astrophysical Journal, Letters*, 516, L1
- Komatsu, E., et al. 2011, *Astrophysical Journal, Supplement*, 192, 18
- Kompaneets, A. S. 1957, *Soviet Phys. — JETP Lett.*, 4, 730
- Kotov, O., & Vikhlinin, A. 2005, *Astrophysical Journal*, 633, 781
- Kravtsov, A. V., Nagai, D., & Vikhlinin, A. A. 2005, *Astrophysical Journal*, 625, 588
- Kravtsov, A. V., Vikhlinin, A., & Nagai, D. 2006, *Astrophysical Journal*, 650, 128
- Laureijs, R., et al. 2011, *ArXiv e-prints*
- Lieu, R., Mittaz, J. P. D., & Zhang, S.-N. 2006, *Astrophysical Journal*, 648, 176
- Limousin, M., Morandi, A., Sereno, M., Meneghetti, M., Ettori, S., Bartelmann, M., & Verdugo, T. 2012, *ArXiv e-prints*
- Lin, Y.-T., Mohr, J. J., & Stanford, S. A. 2003, *Astrophysical Journal*, 591, 749
- Lopes, P. A. A., de Carvalho, R. R., Kohl-Moreira, J. L., & Jones, C. 2009, *MNRAS*, 399, 2201
- Lyutikov, M. 2007, *Astrophysical Journal, Letters*, 668, L1
- Mahdavi, A., Hoekstra, H., Babul, A., Bildfell, C., Jeltama, T., & Henry, J. P. 2012, *ArXiv e-prints*
- Mahdavi, A., Hoekstra, H., Babul, A., & Henry, J. P. 2008, *MNRAS*, 384, 1567
- Mandelbrot, B. 1967, *Science*, 156, 636
- Mantz, A., Allen, S. W., Ebeling, H., Rapetti, D., & Drlica-Wagner, A. 2010a, *MNRAS*, 406, 1773
- Mantz, A., Allen, S. W., Rapetti, D., & Ebeling, H. 2010b, *MNRAS*, 406, 1759

- Markevitch, M. 1998, *Astrophysical Journal*, 504, 27
- Marriage, T. A., et al. 2011, *Astrophysical Journal*, 737, 61
- Marrone, D. P., Smith, G. P., Richard, J., Joy, M., & Bonamente, e. a. 2009, *Astrophysical Journal*, Letters, 701, L114
- Marrone, D. P., et al. 2012, *Astrophysical Journal*, 754, 119
- Maughan, B. J. 2007, *Astrophysical Journal*, 668, 772
- Maughan, B. J., Giles, P. A., Randall, S. W., Jones, C., & Forman, W. R. 2012, *MNRAS*, 421, 1583
- Maughan, B. J., Jones, C., Forman, W., & Van Speybroeck, L. 2008, *Astrophysical Journal*, Supplement, 174, 117
- Maughan, B. J., Jones, L. R., Ebeling, H., & Scharf, C. 2006, *MNRAS*, 365, 509
- McCarthy, I. G., Babul, A., Holder, G. P., & Balogh, M. L. 2003, *Astrophysical Journal*, 591, 515
- McCarthy, I. G., et al. 2010, *MNRAS*, 406, 822
- Melin, J.-B., Bartlett, J. G., Delabrouille, J., Arnaud, M., Piffaretti, R., & Pratt, G. W. 2011, *A&A*, 525,
- Merloni, A., et al. 2012, *ArXiv e-prints*
- Mitchell, R. J., Dickens, R. J., Burnell, S. J. B., & Culhane, J. L. 1979, *MNRAS*, 189, 329
- Mitchell, R. J., Ives, J. C., & Culhane, J. L. 1977, *MNRAS*, 181, 25P
- Mittal, R., Hicks, A., Reiprich, T. H., & Jaritz, V. 2011, *A&A*, 532, A133
- Mohr, J. J. 2002, in *Astronomical Society of the Pacific Conference Series*, Vol. 257, AMiBA 2001: High-Z Clusters, Missing Baryons, and CMB Polarization, ed. L.-W. Chen, C.-P. Ma, K.-W. Ng, & U.-L. Pen, 49
- Morandi, A., Ettori, S., & Moscardini, L. 2007, *MNRAS*, 379, 518
- Muanwong, O., Kay, S. T., & Thomas, P. A. 2006, *Astrophysical Journal*, 649, 640
- Muchovej, S., Leitch, E., Culverhouse, T., Carpenter, J., & Sievers, J. 2012, *Astrophysical Journal*, 749, 46
- Mushotzky, R. F. 1984, *Physica Scripta Volume T*, 7, 157
- Nagai, D., Vikhlinin, A., & Kravtsov, A. V. 2007, *Astrophysical Journal*, 655, 98
- Navarro, J. F., Frenk, C. S., & White, S. D. M. 1995, *MNRAS*, 275, 720
- Novicki, M. C., Sornig, M., & Henry, J. P. 2002, *AJ*, 124, 2413
- O'Hara, T. B., Mohr, J. J., Bialek, J. J., & Evrard, A. E. 2006, *Astrophysical Journal*, 639, 64
- Okabe, N., Zhang, Y.-Y., Finoguenov, A., Takada, M., Smith, G. P., Umetsu, K., & Futamase, T. 2010, *Astrophysical Journal*, 721, 875
- Pacaud, F., Pierre, M., Adami, C., Altieri, B., Andreon, S., & et al. 2007, *MNRAS*, 382, 1289
- Peterson, J. R., Kahn, S. M., Paelers, F. B. S., Kaastra, J. S., Tamura, T., Bleeker, J. A. M., Ferrigno, C., & Jernigan, J. G. 2003, *Astrophysical Journal*, 590, 207
- Piffaretti, R., Arnaud, M., Pratt, G. W., Pointecouteau, E., & Melin, J.-B. 2011, *A&A*, 534,
- Pillepich, A., Porciani, C., & Reiprich, T. H. 2012, *MNRAS*, 422, 44
- Planck Collaboration et al. 2011a, *A&A*, 536, A9
- . 2011b, *A&A*, 536, A7
- . 2011c, *A&A*, 536, A8
- . 2011d, *A&A*, 536, A11
- . 2011e, *A&A*, 536, A12
- . 2012, *A&A*, 543, A102
- . 2013a, *A&A*, 550, A128
- . 2013b, *A&A*, 550, A130
- Pointecouteau, E., Giard, M., & Barret, D. 1998, *A&A*, 336, 44
- Ponman, T. J., Bourner, P. D. J., Ebeling, H., & Böhringer, H. 1996, *MNRAS*, 283, 690
- Ponman, T. J., Cannon, D. B., & Navarro, J. F. 1999, *Nature*, 397, 135
- Ponman, T. J., Sanderson, A. J. R., & Finoguenov, A. 2003, *MNRAS*, 343, 331
- Poole, G. B., Babul, A., McCarthy, I. G., Fardal, M. A., Bildfell, C. J., Quinn, T., & Mahdavi, A. 2007, *MNRAS*, 380, 437
- Popesso, P., Böhringer, H., Brinkmann, J., Voges, W., & York, D. G. 2004, *A&A*, 423, 449
- Pratt, G. W., & Arnaud, M. 2003, *A&A*, 408, 1
- Pratt, G. W., Croston, J. H., Arnaud, M., & Böhringer, H. 2009, *A&A*, 498, 361
- Pratt, G. W., et al. 2010, *A&A*, 511, A85
- Predehl, P., Andritschke, R., Böhringer, H., Bornemann, W., Bräuninger, H., & et al. 2010, in *Society of Photo-Optical Instrumentation Engineers (SPIE) Conference Series*, Vol. 7732, *Society of Photo-Optical Instrumentation Engineers (SPIE) Conference Series*

- Puchwein, E., Sijacki, D., & Springel, V. 2008, *Astrophysical Journal, Letters*, 687, L53
- Randall, S. W., Sarazin, C. L., & Ricker, P. M. 2002, *Astrophysical Journal*, 577, 579
- Rasia, E., et al. 2006, *MNRAS*, 369, 2013
- . 2012, *New Journal of Physics*, 14, 055018
- Reichardt, C. L., et al. 2013, *Astrophysical Journal*, 763, 127
- Reichert, A., Böhringer, H., Fassbender, R., & Mühlegger, M. 2011, *A&A*, 535, A4
- Reiprich, T. H., Basu, K., Ettori, S., Israel, H., Lovisari, L., Molendi, S., Pointecouteau, E., & Roncarelli, M. 2013, *ArXiv e-prints*
- Reiprich, T. H., & Böhringer, H. 2002, *Astrophysical Journal*, 567, 716
- Rephaeli, Y. 1995, *ARA&A*, 33, 541
- Rines, K., Geller, M. J., & Diaferio, A. 2010, *Astrophysical Journal, Letters*, 715, L180
- Rines, K., Geller, M. J., Diaferio, A., & Kurtz, M. J. 2013, *Astrophysical Journal*, 767, 15
- Rines, K., Geller, M. J., Kurtz, M. J., & Diaferio, A. 2003, *AJ*, 126, 2152
- Rosati, P., Borgani, S., Gilli, R., Paolillo, M., & Tozzi, P. 2010, *ArXiv e-prints*
- Rozo, E., Rykoff, E., Koester, B., Nord, B., Wu, H.-Y., Evrard, A., & Wechsler, R. 2011, *Astrophysical Journal*, 740, 53
- Rozo, E., et al. 2009a, *Astrophysical Journal*, 699, 768
- . 2009b, *Astrophysical Journal*, 703, 601
- Rykoff, E. S., et al. 2008a, *Astrophysical Journal*, 675, 1106
- . 2008b, *MNRAS*, 387, L28
- . 2012, *Astrophysical Journal*, 746, 178
- Sayers, J., Czakon, N. G., Bridge, C., Golwala, S. R., Koch, P. M., Lin, K.-Y., Molnar, S. M., & Umetsu, K. 2012, *Astrophysical Journal, Letters*, 749, L15
- Schaye, J., et al. 2010, *MNRAS*, 402, 1536
- Schuecker, P., Böhringer, H., Collins, C. A., & Guzzo, L. 2003, *A&A*, 398, 867
- Shaw, L. D., Nagai, D., Bhattacharya, S., & Lau, E. T. 2010, *Astrophysical Journal*, 725, 1452
- Sheldon, E. S., et al. 2009, *Astrophysical Journal*, 703, 2217
- Short, C. J., & Thomas, P. A. 2009, *Astrophysical Journal*, 704, 915
- Short, C. J., Thomas, P. A., Young, O. E., Pearce, F. R., Jenkins, A., & Muanwong, O. 2010, *MNRAS*, 408, 2213
- Sifon, C., et al. 2012, *ArXiv e-prints*
- Sijacki, D., & Springel, V. 2006, *MNRAS*, 366, 397
- Silk, J., & White, S. D. M. 1978, *Astrophysical Journal, Letters*, 226, L103
- Stanek, R., Evrard, A. E., Böhringer, H., Schuecker, P., & Nord, B. 2006, *Astrophysical Journal*, 648, 956
- Stanek, R., Rasia, E., Evrard, A. E., Pearce, F., & Gazzola, L. 2010, *Astrophysical Journal*, 715, 1508
- Staniszewski, Z., et al. 2009, *Astrophysical Journal*, 701, 32
- Story, K., et al. 2011, *Astrophysical Journal, Letters*, 735, L36
- Sun, M., Voit, G. M., Donahue, M., Jones, C., Forman, W., & Vikhlinin, A. 2009, *Astrophysical Journal*, 693, 1142
- Sunyaev, R. A., & Zeldovich, I. B. 1980, *MNRAS*, 190, 413
- Sunyaev, R. A., & Zeldovich, Y. B. 1970, *Comments on Astrophysics and Space Physics*, 2,
- . 1972, *Comments on Astrophysics and Space Physics*, 4,
- Tozzi, P., & Norman, C. 2001, *Astrophysical Journal*, 546, 63
- Valageas, P., & Clerc, N. 2012, *A&A*, 547, A100
- van Weeren, R. J., Röttgering, H. J. A., Rafferty, D. A., Pizzo, R., Bonafede, A., & et al. 2012, *A&A*, 543, A43
- Vanderlinde, K., et al. 2010, *Astrophysical Journal*, 722, 1180
- Vikhlinin, A., Kravtsov, A., Forman, W., Jones, C., Markevitch, M., Murray, S. S., & Van Speybroeck, L. 2006, *Astrophysical Journal*, 640, 691
- Vikhlinin, A., van Speybroeck, L., Markevitch, M., Forman, W. R., & Grego, L. 2002, *Astrophysical Journal, Letters*, 578, L107
- Vikhlinin, A., Voevodkin, A., Mullis, C. R., van Speybroeck, L., Quintana, H., & et al. 2003, *Astrophysical Journal*, 590, 15
- Vikhlinin, A., et al. 2009a, *Astrophysical Journal*, 692, 1033
- . 2009b, *Astrophysical Journal*, 692, 1060
- Voit, G. M. 2005, *Reviews of Modern Physics*, 77, 207
- Voit, G. M., Bryan, G. L., Balogh, M. L., & Bower, R. G. 2002, *Astrophysical Journal*, 576, 601

- White, M., Hernquist, L., & Springel, V. 2002, *Astrophysical Journal*, 579, 16
- Williamson, R., et al. 2011, ArXiv e-prints, [arXiv:1101.1290](https://arxiv.org/abs/1101.1290)
- Yang, H.-Y. K., Ricker, P. M., & Sutter, P. M. 2009, *Astrophysical Journal*, 699, 315
- Yee, H. K. C., & Ellingson, E. 2003, *Astrophysical Journal*, 585, 215
- Younger, J. D., & Bryan, G. L. 2007, *Astrophysical Journal*, 666, 647
- Zhang, Y.-Y., Finoguenov, A., Böhringer, H., Kneib, J.-P., Smith, G. P., Kneissl, R., Okabe, N., & Dahle, H. 2008, *A&A*, 482, 451
- Zwicky, F. 1933, *Helvetica Physica Acta*, 6, 110